Energy & Environmental Science

ROYAL SOCIETY OF CHEMISTRY

REVIEW

View Article Online
View Journal | View Issue

Cite this: *Energy Environ. Sci.*, 2026, **19**, 1101

Scalable deposition and drying methods toward large-area monolithic perovskite/silicon tandem solar cells

Chenxia Kan,[ab] Chao Luo[b] and Yi Hou *[ab]

Received 8th November 2025,
Accepted 21st January 2026

DOI: 10.1039/d5ee06772c

rsc.li/ees

Monolithic perovskite/silicon tandem solar cells have emerged as a compelling route, combining the certified power conversion efficiencies exceeding 34% for laboratory-scale devices with more cost-effective manufacturing compared to market-established silicon photovoltaics. Despite deployment in pilot processing lines beyond the lab stage, this technology still faces scaling challenges from perovskite sub-cells, such as the incompatibility with contemporary mass production lines and the upscaling efficiency deficit, that are expected to be resolved within a few years to achieve commercial viability. Here, we comprehensively elaborate the scalable deposition and drying methods of perovskite sub-cells on silicon substrates and review their recent advanced progress. We assess the merits and limitations of these competing methods, providing a systematic framework for achieving efficient and durable large-area perovskite/silicon tandem solar cells suitable for industrial production.

Broader context

The global energy transition demands photovoltaic technologies that can break through the efficiency ceiling of conventional silicon, and monolithic PSTSCs have emerged as a leading contender. With lab-scale efficiencies now surpassing 34%, this technology holds immense promise, yet its real-world impact is currently constrained by a critical bottleneck: the lack of established, scalable manufacturing processes for efficient, large-area tandems. This review directly faces this challenge by providing a comprehensive and critical analysis of the core manufacturing issues-scalable deposition and drying methods for the perovskite top cell. We systematically connect key processing strategies with their potential for industrial-scale implementation, covering a broad array of techniques from high-throughput solution-based methods to high-purity vapor-phase and hybrid approaches. Meanwhile, attention is given to the drying stage, examining how drying protocols influence final film quality and device performance. By dissecting the complex trade-offs between device efficiency, process complexity, and industrial compatibility for each pathway, this work serves as an essential roadmap for advancing PSTSC technology toward manufacturable, large-area modules.

1. Introduction

While the practical deployment of photovoltaic technology has long been anchored mainly by single-junction silicon solar cells, this market-mature technology is now approaching its practical efficiency limit,[1,2] prompting the need for solutions to further reduce the levelized cost of electricity. In this context, monolithic perovskite/silicon tandem solar cells (PSTSCs) have emerged as a highly promising candidate, offering a viable pathway not only to surpass the 33.7% Shockley–Queisser efficiency limit of single-junction cells[3] but also to achieve more cost-effective manufacturing.[4] The rapid advancement of this technology is evidenced by a series of efficiency records across progressively larger scales,[5] charting a clear development path from lab to fab: a record laboratory-scale efficiency of 34.85% (1 cm^2 designated illumination area), a certified 33.0% efficiency on commercial M6-sized wafers (260.9 cm^2 aperture area), and a 28.6% efficiency for full-area M10-sized tandem devices. Concurrently, industrial adoption is accelerating with several companies establishing pilot processing lines.[6] A significant milestone was reached in September 2024 when Oxford PV announced it had begun shipping panels incorporating its proprietary perovskite-on-silicon solar cells to U.S. customers for utility-scale installation,[7] strongly indicating that the large-scale industrialization of this transformative technology is imminent.

However, the path to commercializing monolithic PSTSCs is fraught with challenges which originate from the perovskite sub-cell. One of the significant practical hurdles is the

[a] *Department of Chemical and Biomolecular Engineering, National University of Singapore, Singapore 117585, Singapore. E-mail: yi.hou@nus.edu.sg*
[b] *Solar Energy Research Institute of Singapore (SERIS), National University of Singapore, Singapore 117574, Singapore*

incompatibility with established silicon mass production lines. Temperature-sensitive materials within perovskite sub-cells could not stand for the high-temperature thermal budget inherent in standard silicon cell manufacturing, which necessitates a physical and procedural decoupling of the silicon and perovskite sub-cell fabrication lines, not only introducing process integration challenges for high-throughput tandem devices but also presenting a major obstacle to a cost-effective and logistically viable industrial upgrade. Simultaneously, the efficiency deficit upon upscaling, which still remains a critical barrier despite considerable research efforts, can be attributed primarily to increased non-uniformity,[8] shunt paths,[9] series resistance,[10] optical losses[11] and reduced interface and layer reliability[12] over larger areas. It is therefore imperative to identify robust scalable deposition and drying methods to prevent detours in manufacturing upgrades and to expedite the market entry of this technology.

Focusing on scalable deposition and drying techniques for perovskite top cells on silicon wafers, this review systematically explores solution-based, vapor-phase and hybrid deposition methods, as well as versatile drying methods of perovskite films which are applied to large-area production. It synthesizes recent progress to provide a critical analysis of the practicality and inherent challenges of each approach. Finally, we offer a forward-looking perspective on their development trajectories.

2. Scalable deposition methods and their advancements in PSTSCs

While the power conversion efficiencies of PSTSCs have reached impressive heights,[1,13,14] their industrial-scale deployment is currently impeded by the challenge of depositing high-quality, uniform and cost-effective films onto large-area silicon bottom cells. Fabrication protocols perfected in laboratories, most notably spin coating, are incompatible with the economic and throughput demands of mass production. Therefore, a deep understanding of industrially viable deposition technologies is paramount. This chapter delves into the landscape of such scalable methods, offering a comprehensive review of solution-based, vapor-phase and hybrid deposition techniques. For each method, we discuss its fundamental mechanism, highlight key breakthroughs in process optimization and device performance.

2.1. Solution-based deposition

Solution-based deposition methods represent a pivotal route towards the scalable fabrication of monolithic PSTSCs, owing to their low-cost potential, high-throughput capability, compositional flexibility, and adaptability to the topography and fragility of silicon wafers. These techniques are systematically categorized into meniscus-guided coating such as blade coating, doctor-bar (D-bar) coating, and slot-die coating; spray coating; printing technologies such as inkjet printing, screen printing, gravure printing and stamping; as well as reaction-driven deposition like chemical bath deposition, electrodeposition. Most of these methods typically rely on common solvents such as dimethylformamide (DMF), dimethyl sulfoxide (DMSO), *N*-methyl-2-pyrrolidone (NMP), γ-butyrolactone (GBL), which are selected based on their boiling point, vapor pressure, viscosity, surface tension, and chemical compatibility with perovskite precursors and adjacent functional layers.[15] The final film quality and morphology, governed by solvent evaporation dynamics and crystallization kinetics, are strongly influenced by the interplay of environmental conditions, solution chemistry, rheological properties, and microfluidic behavior during drying. Here, we provide a detailed overview of these solution-based deposition strategies, with emphasis on the recent advances tailored to the scalable manufacturing of large-area monolithic PSTSCs.

2.1.1. Meniscus-guided coating. Meniscus-guided coating techniques are prized for their ability to deposit uniform thin films over large and textured substrates while minimizing materials waste.[16,17] Unlike random deposition processes, they harness the predictable physics of a liquid meniscus to exert precise control over wet film coating. As conceptually illustrated in Fig. 1a, meniscus-guided techniques share a common underlying principle: a well-defined, dynamics liquid–gas–solid interface (the meniscus) is formed between a coating head and a substate.[18] As the coating head or substrate translates, it continuously drags a wet film out of the meniscus region, whose characteristics are bridled by a subtle interplay of fluid dynamics, surface chemistry and mass transport.

The physical mechanism of film coating in these techniques can be divided into two distinct regimes as shown in Fig. 1b: the evaporation regime and Landau–Levich regime, whose resulting film thicknesses (h) are highly dependent on the coating speed (V).[19,20] At low coating speeds, the flow of liquid is driven by the need to supplement the liquid lost to solvent evaporation at the meniscus. This makes the evaporation rate (Q_{evap}) at steady state, which equals the flow rate of solvent entering into the meniscus ($Q_{solvent}$), the dominant factor determining the film thickness. Mass conservation dictates that the outward flux of solute from the meniscus (J_{film}) must be compensated by an equal inward flux of solute (J_{solute}) entering the meniscus from precursor ink. Consequently, the film thickness is inversely proportional to the coating velocity, as described below:[19]

$$h = \frac{C}{\rho}\frac{Q_{evap}}{L}V^{-1}$$

where C represents the mass concentration of precursor ink, ρ and L denote the density and width of the deposited solid film, respectively. Although this model might be applied to colloidal solutions like perovskite precursor ink, it is imperative to pay attention to the Marangoni effect of the solute within non-colloidal solutions.[21] In addition, the optimal coating speed in this regime is typically low,[20] which inherently limits high-throughput deposition of perovskite top cells on silicon wafers. To evade this constraint, the coating process must transition to a higher speed domain. As the coating rate surpasses a critical threshold, the generated viscous forces become sufficiently

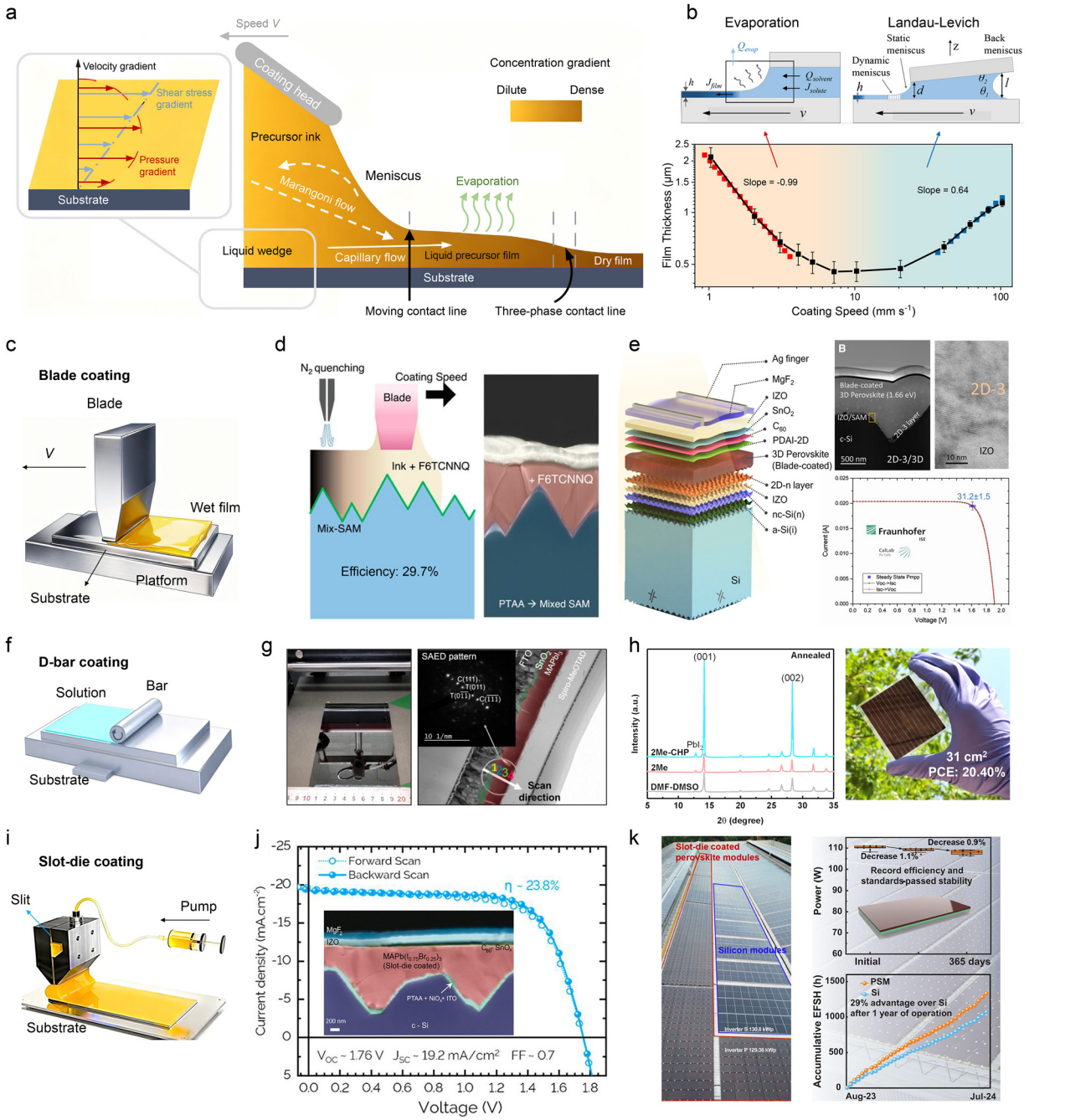

Fig. 1 Meniscus-guided coating methods and their applications in PSTSCs. (a) Schematic diagram of the film forming process and internal flows of the solution during the meniscus-guided coating process. Adapted from ref. 18 with permission from Royal Society of Chemistry,[18] copyright 2025. (b) Schematic of the two deposition regimes in meniscus-guided coating (top) and perovskite film thickness as a function of blade coating speed by coating a precursor ink (bottom). Adapted from ref. 19 with permission from American Chemical Society,[19] copyright 2009. Adapted from ref. 20 with permission from Springer Nature,[20] copyright 2018. (c) Schematic of blade coating. (d) Schematic and cross-section scanning electron microscope (SEM) image of the F6TCNNQ doping PSTSCs with blade-coated perovskites. Adapted from ref. 32 with permission from American Chemical Society,[32] copyright 2024. (e) Device schematic, scanning transmission electron microscope (STEM) images and certified efficiency of blade-coated tandems. Adapted from ref. 16 with permission from Elsevier,[16] copyright 2025. (f) Schematic of D-bar coating. (g) Photo of a D-bar coated $MAPbI_3$ film and related device cross-section TEM image. Inset is selected area electron diffraction pattern showing superlattices of cubic and tetragonal phases. Adapted from ref. 34 with permission from American Chemical Society,[34] copyright 2019. (h) XRD patterns of D-bar coated perovskite films deposited using different solutions and photograph of the D-bar coated perovskite mini-module. Adapted from ref. 35 with permission from Elsevier,[35] copyright 2021. (i) Schematic of slot-die coating. (j) Current–Voltage (*J–V*) curves and cross-section SEM image of slot-die coated PSTSCs. Adapted from ref. 39 with permission from American Chemical Society,[39] copyright 2020. (k) Aerial-view of the rooftop slot-die coated perovskite solar modules (red) and silicon modules (blue), degradation rate of 10 perovskite modules under indoor semiannual standard test condition power output test, and 1-year energy yield of perovskite and silicon modules in term of equivalent full sun hours. Adapted from ref. 8 with permission from The American Association for the Advancement of Science,[8] copyright 2025.

dominant to overcome the capillary forces, thereby initiating the high-speed Landau–Levich regime as depicted. This shift in the modulating fluid dynamics enables significantly higher deposition speed, which is essential for realizing the high yield of large-area PSTSCs. In this regime, the film thickness is confined by the balance between the viscous forces, which resist shearing of the fluid, and surface tension, which seek to minimize the surface area of the liquid, as described by the classic Landau–Levich–Derjaguin (LLD) theory, originally developed from the dip-coating.[22,23] The LLD equation predicts that the wet film thickness is proportional to the coating velocity raised to the 2/3 power and is a function of the capillary number (Ca), a dimensionless number that quantifies the ratio of viscous forces to surface tension:[19]

$$h \propto \mathrm{Ca}^{2/3}, \quad \text{where } \mathrm{Ca} = \frac{\eta \cdot V}{\gamma}$$

Here, η and γ are the viscosity and surface tension of the precursor ink. Understanding the transition between these two regimes is necessary for process control, as the optimal coating speed must be selected to ensure uniform film thickness and proper crystallization kinetics.

Beyond the initial wet film coating, the progression to a solid film involves a critical drying and crystallization stage for perovskite film deposition. This phase is dictated by solvent evaporation dynamics. As the solvent evaporates from the wet film, the precursor concentration increases, eventually reaching supersaturation that triggers nucleation and crystal growth.[24] The evaporation rate, is influenced by factors like substrate temperature,[25] ambient pressure,[8] and gas flow termed gas knife or gas quenching,[26] is a critical parameter. A rapid evaporation rate can produce a high density of nucleation sites, leading to small, densely packed grains, but it may trap residual solvent or induce film cracking. Conversely, a slow evaporation rate facilitates the growth of larger, more ordered crystals but carries the risk of incomplete surface coverage[27] and dewetting. Recent research has therefore focused on involuted solvent engineering, using mixtures of solvents with different physicochemical properties or incorporating additives to fine-tune crystallization kinetics and passivate defect.[16,28,29] These strategies enable the fabrication of high-quality perovskite films even at industrial-scale coating speeds. The capacity to precisely manage these intertwined fluid dynamics and crystallization is what establishes meniscus-guided coating as a powerful platform for manufacturing large-area monolithic PSTSCs.

Blade coating. Blade coating, often referred to as knife coating, is a quintessential meniscus-guided, pre-metered deposition technique in which a blade or squeegee translates at a fixed height above the substrates, shearing the solution in front of the blade and then leaving behind a wet film, as shown in Fig. 1c. The thickness of this film is primarily determined by the blade gap height, coating speed, and ink rheology, operating in either the evaporation or Landau–Levich regime. However, achieving high thickness uniformity presents a fundamental challenge. The process is highly dependent on maintaining a constant advancing meniscus height. As the solution is consumed during coating, the meniscus is dynamic, leading to a corresponding reduction in film thickness along the coating direction and resulting in gradients.[30] This uniformity is sensitive to process parameters such as substrate temperature, dispensed solution volume, and coating speed, requiring precise control to minimize capillary flow and thickness variation. Despite this inherent challenge, blade coating remains a simple, low-cost method capable of high throughput, excellent material utilization, and adaptation to large-area, textured substrates or roll-to-roll (R2R) formats.

In the context of monolithic PSTSCs, blade coating has demonstrated remarkable performance by integrating advanced strategies that gradually enhance the efficiency and also alleviate the inhomogeneity concerns. Chen *et al.* developed an architecture that integrated a conformal hole transport layer (HTL) and a dense planarizing perovskite layer on silicon cells with submicrometer pyramidal textures at first time by using nitrogen-assisted, meniscus-guided blade coating method.[31] With a textured front polydimethylsiloxane antireflection coating, a diminished pyramid size less than 1 μm in height and an optimized perovskite solvent system of 2-methoxyethanol/DMF/DMSO, they achieved a 26% efficiency. In another work, by integrating molecular p-doping with 2,2′-(perfluoronaphthalene-2,6-diylidene)dimalononitrile (F6-TCNNQ) and employing a mixed self-assembled monolayer (SAM)-based hole-selective layer (Fig. 1d), blade-coated PSTSCs achieve an efficiency of 29.7%, demonstrating the effectiveness of combined material and interface engineering in meniscus-guided methods.[32] Subbiah *et al.* utilized blade coating of a perovskite ink with dimethyl-2-imidazolidinone (DMI)/DMF solvents to deposit three-dimensional (3D) perovskite onto a two-dimensional (2D) perovskite film made prior to the 3D layer (Fig. 1e). By introducing 2D/3D heterojunctions at the upper and buried interfaces of the perovskite absorber, an independently certified efficiency of 31.2% within 1 cm^2 area for blade-coated tandem was demonstrated.[16] Moreover, advancements in process control directly target uniformity challenges. Research has shown that actively modulating the coating meniscus by precisely adjusting a co-flowing gas stream could stabilize the meniscus shape, control solvent evaporation, and yield large-area perovskite films with exceptional uniformity, high crystal orientation, and reduced strain. This meniscus modulation technique effectively counters the inherent thickness gradients, enabling the fabrication of efficient perovskite solar minimodules.[26] Furthermore, strategies like strain-release post-treatment have been developed to mitigate the top-down inhomogeneity strains prevalent in blade-coated perovskite films, enhancing both efficiency and operational stability for tandem applications.[33] These results prove that blade coating is a viable technique for high-efficiency, industrially scalable deposition of all layers within perovskite cells, though achieving long-term stability on monolithic PSTSCs continues to be a vital exploration.

D-bar coating. D-bar coating is a simplified variant of blade coating, in which a fixed bar deposits a wet film as either the

substrate or the bar moves, as depicted in Fig. 1f. The wet film thickness is controlled by the gap, bar geometry, substrate speed and ink properties. This technique provides a straightforward yet effective way to achieve discrete and highly reproducible film thicknesses without requiring precise gap control between the bar and the substrate. During coating, the bar remains in direct contact with the substrate, pushing the excess ink forward while leaving a metered layer behind. The crystallization is then controlled by subsequent drying and annealing procedures. The simplicity and low cost of D-bar coating make it exceptionally well-suited for high-throughput, large-area manufacturing.

Although no studies have yet reported the fabrication of monolithic PSTSCs by this method, D-bar coating has been successfully applied to the scalable production of perovskite solar modules. Jeong *et al.* synthesized pre-formed perovskite clusters within precursor ink *via* a gas-mediated solid–liquid conversion to deposit $MAPbI_3$ films by D-bar coating, enabling perovskite films over an area exceeding 100 cm^2 to exhibit tetragonal/cubic superlattice structures with a highly preferred orientation, as shown in the selected area electron diffraction pattern (Fig. 1g).[34] Additionally, mini-modules fabricated using 2-methoxyethanol as a solvent and *n*-cyclohexyl-2-pyrrolidone as an additive to balance the nucleation and crystal growth, combined with surface treatment using acetylcholine bromide, attained an efficiency of 20.40% with a preferred perovskite crystal orientation (Fig. 1h).[35] In other studies, D-bar coating was also employed to deposit 2D Ruddlesden–Popper perovskite films and to conformally coat compact TiO_2 layers on FTO glass.[36,37] However, as the area increases, the process window narrows. In brief, the ability of D-bar coating to rapidly produce uniform films with minimal material waste is critical for the economic scalability of PSTSC manufacturing, but it requires more precise research and development to achieve this goal.

Slot-die coating. Slot-die coating is a highly precise, premetered deposition method ideal for large-scale, continuous manufacturing. In this process, the precursor ink is pumped at a constant flow rate through a narrow, precision-machined slit in a coating head, forming a liquid curtain or meniscus onto the moving substrate (Fig. 1i).[38] A stable ''coating bead'' of liquid is maintained between the two lips of the slot-die head and the substrate. The upstream meniscus of the bead contains the liquid, while the downstream meniscus defines the deposited wet film. The final film thickness is precisely controlled by the ink flow rate, the coating speed, the width of the slot and the mechanical gap between head and substrate, which allows for extremely uniform films over very large areas, even on non-planar or flexible substrates. Renowned for its high material utilization, minimal waste, and compatibility with high-speed R2R processing, slot-die coating is considered one of the most promising methods for scaling-up perovskite-based photovoltaics.

As a forefront of efforts to scale up perovskite-based solar cells from the lab to the fab, the application of slot-die coating for monolithic PSTSCs remains in its early stages, with published reports being notably limited. The first breakthrough was reported by Subbiah *et al.* who integrated perovskite films with acetonitrile/methanol solvent and a surfactant, l-α-phosphatidylcholine as an additive followed by surface passivation treatment of cysteine hydrochloride on textured silicon, achieving the first slot-die coated perovskite/silicon monolithic tandems with an efficiency of 23.8% (Fig. 1j).[39] By using a tailored solvent system, N_2-knife drying and optimized annealing conditions to slot-die coat triple-halide perovskite films on saw damage etched commercial Czochralski (Cz) wafers, a 25.2% efficiency was demonstrated with fully scalable processes.[40] Qiang *et al.* slot-die coated the perovskite absorber with FAI and mF-PEAI to eliminate excess PbI_2 and passivate surface defect, improving the efficiencies up to 28.68% and 24.22% for PSTSCs of 1 cm^2 and 14.44 cm^2 areas, respectively.[29] This year, Geistert *et al.* improved the homogeneity of drying process within 2-step slot-die coating *via* a new 2D comb-nozzle drying technique, integrating homogeneous and pinhole-free large-area perovskite on silicon bottom cells with 24.6% efficiency of large-area tandems.[41] It is worth noting that groundbreaking progress is being made in the flexible counterparts with slot-die coated perovskite layers. The M6-sized flexible device achieved a certified efficiency of 29.8% (261.14 cm^2) by developing a dual-buffer layer architecture with a stress-release mechanism, which not only confirms the successful application of this scalable technology in large-area PSTSCs but also highlights its great advantage on flexible substrates.[42]

Although reports on slot-die coating for PSTSCs are limited, it has been extensively studied for single-junction perovskite solar cells (PSCs).[43–45] Bu *et al.* used slot-die coating to scale up perovskite absorber deposition, combining NMP adduct formation to promote the formation of the desired black α-phase at room temperature and KPF_6 interface passivation, achieving 20.4% efficiency in a 17 cm^2 module while eliminating hysteresis and improving thermal stability.[44] In a recent work, by slot-die coating tin oxide nanocrystal ink with poly(acrylic acid), flexible PSCs and modules with fully slot-die coated functional layers achieved high efficiencies of 22.46% (0.1486 cm^2) and 16.4% (30 × 30 cm^2) along with excellent mechanical bending and storage stability.[46] This year, Yan *et al.* built a 0.5-megawatt peak power perovskite solar farm with 0.7906-m^2 slot-die coated perovskite solar modules (Fig. 1k), and implemented a 1-year operational study which indicated a 29% higher energy yield per kilowatt of installed capacity compared with that of silicon modules at the same facility owing to low temperature coefficients.[8] With a 2% degradation at the first year and projected 9-year T_{90} lifespan, these results advanced single perovskite commercialization and implied a promising future for slot-die coated perovskite-based devices including large-area monolithic PSTSCs.

However, achieving film quality comparable to that of small-area spin-coated films remains challenging, especially when depositing on textured silicon bottom cells. While significant progress has been made in device performance, the highest tandem efficiencies are still often obtained using spin-coating method. The technique nevertheless holds excellent scalability

potential and benefits from relatively low cost compared with vacuum-phase deposition methods, which makes it attractive for mass production of PSTSCs. Key challenges include ensuring complete infiltration of the wet film into textured geometric structures, maintaining homogeneous drying, nucleation and crystallization across wide coating widths and long depositing length to avoid thickness gradients, voids, or other defects. Furthermore, integrating high-speed drying, ensuring process robustness, and maintaining yield and operational stability over large areas remain critical for commercialization, as the process window narrows with increasing device size. Overall, slot-die coating stands as a leading candidate for large-area tandem fabrication, but sustaining film quality and reliability at industrial scale is essential to fully realize its potential.

The advancements mentioned above indicate that the continued refinement of meniscus-guided coating processes and ink engineering is critical to achieving cost-effective, high-throughput manufacturing of monolithic large-area PSTSCs. Thus, a comparative mechanistic analysis of meniscus-guided coating techniques, which highlights distinct approaches to film uniformity, is necessary for scaling up production. Blade coating utilizes an open meniscus with solution fed from a reservoir in front of the blade, making uniformity particularly sensitive to fluctuations in solution volume and meniscus stability. D-bar coating, which is often considered similar, operates with a fixed gap that meters the film but faces similar challenges from edge effects and meniscus dynamics. In contrast, slot-die coating employs a closed, pressurized system that feeds ink directly into a precision slot, creating a more confined and stabilized upstream meniscus. This design allows for better control over flow distribution and minimizes external perturbations, typically resulting in superior thickness uniformity and a broader operational coating window for stable deposition. While slot-die coating is preferred for large-area, continuous production due to its enhanced uniformity, blade coating still holds advantages in terms of operational simplicity, ease of cleaning, and lower equipment costs, making it highly suitable for rapid exploration and certain scalable applications. In addition, hybrid technology of combining evaporation with meniscus-guided coating will be introduced later.

2.1.2. Spray coating. Spray coating represents another promising scalable deposition technique for large-area perovskite thin films. Its ability to deposit uniform coatings on complex or non-planar surfaces, such as the textured silicon bottom cells used in monolithic perovskite/silicon tandems, makes it particularly attractive for industrial implementation. Unlike meniscus-based methods, spray coating relies on the atomization of a precursor ink into fine droplets, which are then directed toward the substrate with non-contact mode by a carrier gas as shown in Fig. 2a.[47,48] The detailed sequence can be broken into four successive stages:

(i) Droplet generation (atomization). A precursor solution is forced through a nozzle with pneumatic, ultrasonic spraying or electro-spraying and broken into droplets. The droplet diameter, velocity, and uniformity depend on nozzle geometry, solution viscosity, surface tension, flow-rate and gas/air pressure.

(ii) Droplet transport and impingement on the substrate. The droplets travel through a gas stream and impinge on the substrate. The wetting of each droplet depends on solution contact angle, substrate temperature, and Marangoni flows. Good wetting and fast spreading favor uniform coalescence.

(iii) Coalescence and film formation. At sufficient droplet impingement density, droplets merge to form a continuous wet film. If too sparse or too slow, the film may develop dry patches, non-uniform thickness, or ''coffee-ring'' effects.

(iv) Solvent evaporation and crystallization. As the solvent evaporates, supersaturation triggers crystallization of the film. The drying dynamics, such as evaporation rate, substrate temperature, gas quenching and nucleation/growth kinetics govern film morphology. For spray coating, controlling the drying kinetics is critical: rapid evaporation can lead to inhomogeneous films, pinholes, cracked morphology or incomplete conversion, whereas slower drying may promote larger grains but risk dewetting or non-uniformity.

While much of the literature focuses on single-junction PSCs, there are emerging works applying spray coating to monolithic PSTSCs. Chen *et al.* proposed a surface reconstruction strategy by depositing a bifunctional molecule, fluorinated thiophenethylammonium onto the surface of perovskite film *via* a dynamic spray coating technique (Fig. 2b), resulting in a conformal, dipole passivation layer coatings, which enabled the monolithic PSTSCs to achieve a certified efficiency of 30.89%.[49] One notable study adapted spray coating alumina particles onto fully textured silicon with over 2–4 μm pyramids (Fig. 2c), creating a super-hydrophilic rough surface that both enhances wet film coverage and provides guided nucleation sites, which obtained a tandem efficiency of 32.74%.[50] Graded $CsPbI_{3-x}Br_x$ thin film was integrated into a perovskite submodule by a scalable, orthogonal processable spray coating approach, demonstrating a 13.82% efficiency over a 112 cm^2 aperture area.[51] Furthermore, ultrasonic spray and electrospray have also been applied in PSCs.[52,53]

These progresses indicate that spray coating as a non-contact, scalable deposition method, is well-suited for fragile or textured silicon surfaces, offering conformal coverage and high throughput. It has been applied to large-area and flexible perovskite or tandem devices, but achieving uniform, defect-free, and highly crystalline films remains difficult. Challenges include material waste, complex drying behavior, and limited process control over large areas. Despite these limitations, spray coating remains attractive for low-cost, high-throughput manufacturing, particularly for flexible or fluctuant substrates, though significant improvements in film quality and crystallization control are required for efficient large-area monolithic PSTSCs.

2.1.3. Printing technology. Printing technologies offer unparalleled advantages in digital control, material efficiency, and potential for high-throughput, large-area fabrication with encompassing a broader set of mechanism for transferring functional inks onto substrates. Among the printing methods, non-contact inkjet printing stands out with its ability to deposit defined volumes of precursor ink, enabling digital patterning,

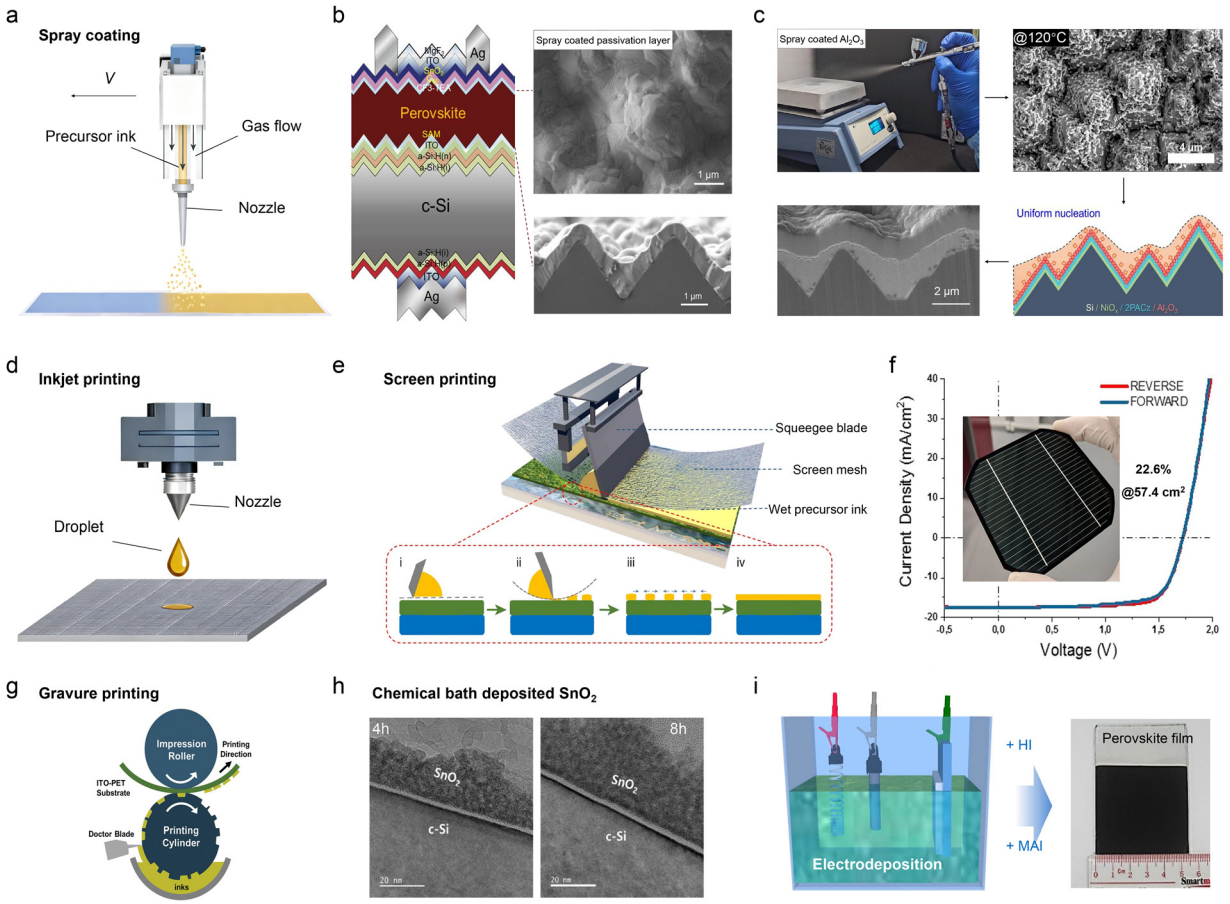

Fig. 2 Schematic of Spray coating, printing technologies and reaction-driven deposition and their applicants. (a) Schematic of spray coating. (b) Schematic illustration of a PSTSC, top-view and cross-section SEM images of perovskite films with spray coated fluorinated thiophenethylammonium passivator on the perovskite films. Adapted from ref. 49 with permission from John Wiley and Sons,[49] copyright 2024. (c) Spray coated Al_2O_3 suspension for particle decoration of the surface of textured silicon. Adapted from ref. 50 with permission from Springer Nature,[50] copyright 2025. (d) Schematic of inkjet printing. (e) Schematic of screen printing. Adapted from ref. 64 with permission from Springer Nature,[64] copyright 2022. (f) *J*–*V* curves and a photo of a large-area PSTSC with screen printed silver paste. Adapted from ref. 68 with permission from American Chemical Society,[68] copyright 2019. (g) Schematic diagram of gravure printing on the flexible substrate. Adapted from ref. 70 with permission from John Wiley and Sons,[70] copyright 2019. (h) TEM images of the chemical bath deposited SnO_2 on silicon bottom cells. Adapted from ref. 76 with permission from MDPI,[76] copyright 2021. (i) Electrodepositing PbO_2 for perovskite film fabrication. Adapted from ref. 79 with permission from Elsevier,[79] copyright 2015.

minimal waste, and potential compatibility with R2R and mechanically sensitive fragile silicon wafers. Meanwhile, screen printing as a workhorse for its established role in metallization will be evaluated. Methods like gravure printing or stamping are also briefly mentioned.

Inkjet printing. Inkjet printing is a fully digital, non-contact deposition method where precise, picoliter-sized droplets of precursor ink are ejected from a printhead nozzle onto a substrate (Fig. 2d). Compared with other printing technologies, the digital and non-contact nature are its most significant advantages for tandem applications, as it localizes film deposition and eliminates mechanical stress on the fragile textured silicon substrate, thereby minimizing materials waste and the risk of micro-cracks occurred within silicon wafers. There are two primary modes of inkjet printing:[54]

(1) Continuous inkjet. A continuous stream of droplets is generated, and an electric field deflects unwanted droplets into a gutter for recirculation. This process is extremely fast but is more complex.

(2) Drop-on-demand (DOD). Droplets are ejected from the nozzle only when required. This is typically achieved *via* thermal or piezoelectric actuators. Piezoelectric DOD is the dominant method for functional-material printing, as it avoids heating the ink, making it compatible with thermally sensitive perovskite precursors.[55] During this process, the droplet formation sequence typically goes through several key stages: the liquid is first ejected and elongated, then a slender filament detaches from the nozzle exit, after which the filament contracts, fragments into a main droplet plus one or more smaller satellite droplets, and occasionally the satellites merge back into the primary droplet.[56]

For successful inkjet printing of films, the "printability" of the ink is paramount. This is primarily determined by the *Z* number, defined as the reciprocal of the Ohnesorge number (Oh), which itself relates the inertial (*via* the Reynolds number,

Re) and capillary (*via* the Weber number, We) and viscus forces in the fluid:[57]

$$Z = {}^{1}/_{\mathrm{Oh}} = \frac{\mathrm{Re}}{\mathrm{We}^{1/2}} = \frac{(\gamma\rho\alpha)^{1/2}}{\eta}$$

where γ is the surface tension, ρ is the fluid density, α is the characteristic length such as the diameter of the jetting nozzle and η is the fluid viscosity. A stable drop formation without satellites or splashing is typically achieved for $1 < Z < 10$.[58] This requires careful formulation of the ink by tuning its viscosity, surface tension, and solvent composition. Upon deposition, the coalescence of droplets and subsequent crystallization kinetics determine the final film quality. The coffee ring effect is a major challenge that can lead to non-uniform film thickness and morphology, which can be mitigated through strategies such as optimizing substrate temperature, controlling solvent evaporation rates, or printing in a saturated solvent vapor atmosphere.

The application of inkjet printing in monolithic PSTSCs is particularly promising for addressing one of the most formidable challenges: conformal deposition on textured silicon.[59] This year, perovskite manufacturer Phenosolar has launched its new inkjet research & development production line for tandem solar cells, equipped with high-precision inkjet testing equipment, screen printing, and more.[60] In addition, inkjet printing technology has made significant advancements in the fabrication of perovskite single-junction solar cells, encompassing the deposition of both the perovskite layers and the charge extraction layers.[61–63]

That means, inkjet printing offers digital, maskless, and selective material deposition with excellent spatial control and minimal waste, making it useful for patterned fabrication in PSTSCs. However, for large-area deposition, droplet coalescence and non-uniform crystallization often degrade film quality and device performance. Although this method minimizes material loss, equipment and maintenance cost, and low-throughput hinder its industrial adoption. Overall, inkjet printing shows potential for precise, localized coating in monolithic PSTSCs, but achieving uniform, high-quality films over large-area textured silicon surfaces remains a challenge for scalable manufacturing.

Screen printing. Screen printing is a mature, low-cost, scalable and high-throughput deposition technique widely used in the established photovoltaic industry, particularly for thick metal electrodes. This technique involves three main components: a patterned screen mesh (typically of stainless steel, coated with an emulsion to block off non-printing areas), a viscous ink, and a squeegee blade (Fig. 2e).[64] The process unfolds as follows:[65]

(i) The substrate is placed beneath the screen at a small distance known as the ''snap-off'' distance.

(ii) A flood squeegee applies a layer of ink onto the screen.

(iii) The squeegee moves across the screen, applying downward pressure. This pressure flexes the screen to make momentary contact with the substrate.

(iv) As the squeegee passes, it forces the ink through the open areas of the screen onto the substrate.

(v) The screen then ''snaps off'' the substrate due to its elasticity, leaving the printed pattern behind. The printed film is subsequently post-treated.

However, its resolution is limited by the mesh size and ink rheology, and thus lower than inkjet printing. While challenging for depositing high-quality, thin perovskite absorber layers due to this resolution limitations, it has still found applications in perovskite single-junctions. With a stable and viscosity-adjustable perovskite ink from a methylammonium acetate ionic liquid solvent, the PSCs with screen-printed perovskite layer or all functional layers exhibited efficiencies of 20.52% or 14.98%.[64] By introducing another ionic liquid methylamine propionate with stronger coordination to promote the volatilization of solvent, they further enhanced the efficiency up to 17% of fully screen-printed PSCs.[66] The first screen-printed flexible PSCs with 18.6% efficiency and good mechanical stability also be fabricated this year.[67] For tandem devices, Kamino *et al.* demonstrated a low-temperature silver paste applied by screen printing for the front metal grid of monolithic PSTSCs, achieving a steady-state efficiency of 22.6% over an aperture area of 57.4 cm^2 with a two-bus bar metallization pattern (Fig. 2f)[68]. Additionally, fine line screen printing for the device metallization and interconnection has been integrated into full-sized, monolithic PSTSCs and modules.[69] These results demonstrate the potential of screen printing for the realization of large-area monolithic tandems, primarily for metal electrodes.

Gravure printing and stamping. Gravure printing is a high-speed R2R process where an engraved cylinder transfers ink from its cavities to a substrate (Fig. 2g).[70] It is excellent for high-resolution patterning and has been explored for printing PSCs.[71,72] However, like screen printing, it is a contact-based method that applies pressure, making it inherently less suitable for fragile silicon wafers. Its potential lies in depositing layers on flexible substrates or in mechanically insensitive architectures.

Stamping involves picking up a pre-formed material from a donor substrate and transferring it to a target substrate. It offers excellent control over crystal orientation and can be used to create complex heterostructures. While useful for fundamental studies and perovskite devices,[73–75] the challenge of achieving uniform contact and release over large areas, combined with the associated mechanical stresses, currently limits its practicality for large-area monolithic PSTSC fabrication.

In brief, printing technology offers a versatile strategy for fabricating PSCs. Inkjet printing is particularly well-suited for monolithic PSTSCs, while screen printing remains a scalable option for electrode deposition. The main driver force for progress has been the development of specialized inks with optimized physicochemical properties, paving the way for large-area PSTSCs manufacturing.

2.1.4. Reaction-driven deposition. In addition to the solution-based methods mentioned above, which deposit a pre-formed precursor film followed by solvent evaporation

and crystallization, a distinct class of reaction-driven deposition techniques, such as chemical bath deposition (CBD) and electrodeposition (ED), have also been applied in perovskite-based solar cells. This type of approaches relies on *in situ* chemical reactions occurring at the substrate-solution interface or within a solution bath, thereby forming the films by nucleation and growth directly on the substrates. With the advantages of conformal coverage, low-temperature processing, and good adaptability to textured substrates, reaction-driven deposition technologies have also been developed in PSTSCs. A recent work applied a low-temperature CBD-deposited SnO_2 electron transport layer (ETL) on a silicon bottom cell (Fig. 2h) for monolithic perovskite/silicon tandem configuration, achieving a tandem efficiency of 16.9% and indicating the feasibility of CBD on large-area silicon surfaces.[76] Although the direct application of ED in monolithic PSTSCs has not been reported, several relevant developments have been demonstrated in single-junction PSCs for the deposition of perovskite layers (Fig. 2i) and charge transport layers.[77–79]

However, despite their conceptual appeal, low cost, scalability, and established industrial use for oxide and semiconductor films, the adaptation of these methods to hybrid perovskite materials remains at an early stage. It is difficult to manage the complex conversion kinetics of halide perovskites and ensure compatibility with textured silicon surfaces and tandem interfaces. Overall, reaction-driven deposition represents a potentially low-cost and scalable alternative, but achieving the high film quality, device efficiency, and long-term stability required for large-area monolithic PSTSCs will demand substantial further development.

In summary, solution-based deposition techniques provide a versatile and scalable platform for fabricating the perovskite top cells in monolithic tandems. From meniscus-guided and spray coating to printing and *in situ* reaction-driven methods, these approaches offer compelling pathways for low-cost, scalable, high-throughput manufacturing.

2.2. Vapor-phase deposition

Vapor-phase deposition techniques represent a mature and scalable approach for fabricating thin-film photovoltaics. These techniques, featured solvent-free processing, superior film uniformity and stability, better compatibility with industrial processes, offer unparalleled control over film stoichiometry, thickness, and conformality particularly on the textured surfaces. Here, vapor-phase methods are broadly categorized into physical vapor deposition (PVD) and chemical vapor deposition (CVD), with the former relying on physical transformations and the latter on chemical reactions for film formation. This section systematically reviews the mechanisms and recent advances in key vapor-phase techniques, including thermal evaporation, close space sublimation, continuous flash sublimation, sputtering, chemical vapor deposition, highlighting their application in large-area tandem devices.

2.2.1. Physical vapor deposition

Evaporation. Thermal evaporation operates under high vacuum conditions (typically $<10^{-4}$ Pa), where source materials are heated to their sublimation temperatures, generating vapor species that travel ballistically to condense on a substrate. The process allows precise control over evaporation rates, substrate temperature, and deposition sequence *via* conventional thermal evaporation, close space sublimation (CSS) and continuous flash sublimation (CFS). Evaporation techniques have been widely employed for the deposition of metal electrodes, charge transport layers and interfacial layers, while for perovskite deposition, two primary configurations are employed:[80]

(1) Co-evaporation (Fig. 3a). Simultaneous evaporation of multiple precursors from independently controlled sources like heated crucible, enabling real-time, precise control over complex stoichiometries.

(2) Sequential evaporation (Fig. 3b). Precursor layers are deposited one after another. A subsequent thermal annealing step is required to promote interdiffusion and drive the solid-state reaction to form the functional layers. This approach simplifies process control by decoupling the deposition of each component.

For the applications of these two evaporation modes in PSTSCs, researchers have successfully employed co-evaporation to deposit $MAFAPbI_3$ perovskite on silicon bottom cells (Fig. 3c), obtaining the first fully textured monolithic PSTSC with a co-evaporated perovskite absorber that reached an efficiency of 24.6%.[81] Meanwhile, the single-junction PSCs maintained 99% initial efficiency after 1000 h maximum-power-point tracking. This year, with a molecular recombination junction composed of an n-doped C60 layer and a p-doped conjugated arylamine layer, PSTSCs with fully evaporated perovskite top cells enable an efficiency above 22%.[82] Our group also reported a work that exhibited a projected $\sim$70 000 h operational stability and outstanding thermal resistance of co-evaporated PSCs with a self-guided crystal-growth mode *via* intermediate phase evolution (Fig. 3d).[83] Another study reported a reverse layer-by-layer deposition strategy to control the diffusion of solid-phase precursor (Fig. 3e), whereby the organic FAI was deposited before the inorganic precursors, achieving 25.19% efficiency for the sequential evaporated single-junction PSCs with 95.2% initial efficiency after 1000 h operation.[84] So many researches have implied that evaporation technology might be widely used in the future fabrication of the durable perovskite layers.

In addition to the conventional thermal evaporation technology, CSS is a thermally-driven PVD technique engineered for high-rate, large-area deposition (Fig. 3f).[85] The precursor source and the substrate are placed in very close proximity (microns to millimeters apart) within a chamber backfilled with low-pressure inert gas. The source is heated to a high temperature, causing rapid sublimation. The short distance and the presence of the background gas create a viscous flow regime, allowing vapor to transport rapidly and efficiently to the cooler substrate. This minimizes material loss and enables deposition rates orders of magnitude higher than conventional evaporation. CSS has been successfully used to deposit high-quality perovskite films with excellent uniformity,[85–87] positioning it as a

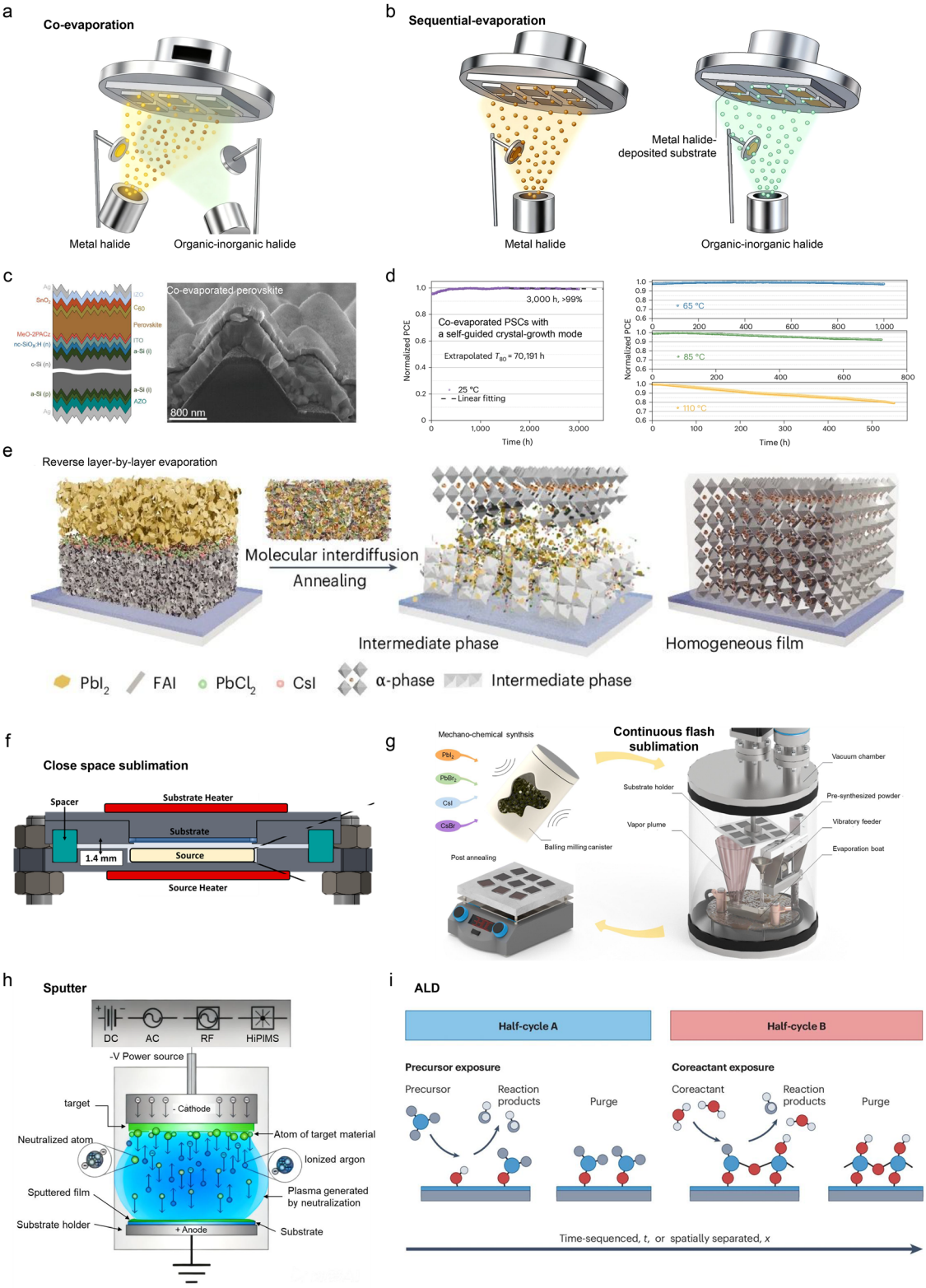

Fig. 3 Schematic of vapor-phase deposition methods and their applicants. (a) Co-evaporation and (b) sequential evaporation. Adapted from ref. 80 with permission from Springer Nature,[80] copyright 2025. (c) Schematic and SEM image of fully textured PSTSCs with co-evaporated perovskite layers. Adapted from ref. 81 with permission from John Wiley and Sons,[81] copyright 2021. (d) Normalized maximum power point tracking stability at different temperatures of PSCs with co-evaporated perovskite films *via* the self-guided crystal-growth mode. Adapted from ref. 83 with permission from Springer Nature,[83] copyright 2025. (e) A crystallization mechanism of sequential evaporation from solid precursor to perovskite. Adapted from ref. 84 with permission from Springer Nature,[84] copyright 2025. (f) Solidworks cross section of the close space sublimation chamber. Adapted from ref. 85 with permission from American Chemical Society,[85] copyright 2024. (g) Schematic illustration of the continuous flash sublimation system. Adapted from ref. 88 with permission from Royal Society of Chemistry,[88] copyright 2024. (h) Direct-current magnetron sputtering process. Adapted from ref. 89 with permission from Elsevier,[89] copyright 2019. (i) Schematic of an ALD cycle in which a surface is alternately exposed to a precursor (step A) and a coreactant (step B). Adapted from ref. 95 with permission from Springer Nature,[95] copyright 2025.

promising technology for cost-effective, high-throughput industrial manufacturing, which is potential for the fabrication of PSTSCs.

CFS is an innovative technique designed to safely deposit thermally unstable or incongruent materials (Fig. 3g).[88] Instead of heating a bulk source material, which can lead to decomposition over time, CFS involves continuously feeding fine precursor microparticles into a flash-heating zone. The particles sublimate almost instantaneously upon entering this high-temperature zone. An inert carrier gas then transports the resulting vapor to the substrate. This "flash" sublimation minimizes the time the precursor spends at high temperature, effectively preventing thermal decomposition. This method opens a pathway for depositing complex, multi-component perovskite compositions that are otherwise inaccessible *via* conventional evaporation, making it a technology for exploring new material systems in a scalable manner towards PSTSCs.

Evaporation-based deposition techniques have been long established in thin-film photovoltaics owing to their precise control over film stoichiometry, thickness, and uniformity. These methods enable highly uniform, conformal, and compositionally controlled films even on textured silicon surfaces, although their stringent processing conditions make it challenging to incorporate bulk additives and passivators. While fully evaporated tandem devices currently deliver slightly lower efficiencies than solution-processed counterparts, they exhibit excellent stability, as demonstrated in single-junction PSCs, underscoring their long-term potential. Despite their maturity and high film quality, evaporation processes face significant limitations in scalability and cost: large-area deposition requires expensive vacuum equipment, high energy consumption and long processing times, constraining throughput. Thus, future progress must focus on improving process efficiency, reducing costs, and enabling integration with high-throughput manufacturing to make vacuum-based deposition a viable route for scalable, large-area monolithic PSTSCs.

Sputter. Sputtering is a PVD technique where a plasma, typically argon ions, is generated to bombard a target material, ejecting atoms or cluster that then travel through the vacuum and condense onto a substrate to form a film (Fig. 3h).[89] During this process the film growth mechanism involves adatom arrival, surface diffusion, nucleation, and coalescence, and the film properties such as thickness, density, crystallinity, and interface quality, that can be tuned by adjusting parameters such as ion energy, gas pressure, target-substrate distance, and substrate temperature.[90] The resulting films are typically dense, with strong adhesion, making this technique suitable for large-area fabrication.

In PSTSCs, it is extensively used for depositing transparent conductive oxides (TCOs) like ITO, metal electrodes and charge transport layers. A sputtered TCO can serve as a recombination or interconnecting layer, enabling high-efficiency monolithic integration *via* careful control of deposition mechanics, interfacial engineering, stress and damage mitigation. Besides, Hou *et al.* deposited nanocrystalline NiO_x by sputtering as the HTL on the top of the recombination junctions of PSTSCs.[91] Aydin *et al.* developed sputtered amorphous niobium oxide with evaporated ligand-bridged C60 as an efficient electron transport layer on the textured silicon bottom cells.[92] While its use for perovskite deposition is limited due to potential damage from high-energy particles and low quality of films, there still are works that introduced sputtering into single-junction PSCs for the sputtered PbI_2 templates.[93,94]

To sum up, this technique provides good film uniformity and conformal coverage over large areas and can effectively coat textured substrates, showing strong potential for scalable production. However, due to the damage of the energetic particles involved in sputter, a pre-deposited buffer layer is necessary. Meanwhile, the sputtered deposition of perovskite remains pessimistic. Therefore, although the cost of sputtering varies depending on target materials and equipment, its excellent industrial compatibility makes it particularly suitable for the deposition of TCOs and charge transport layers in monolithic PSTSCs.

2.2.2. Chemical vapor deposition. CVD represents a powerful class of techniques where volatile precursors react on a heated substrate to form a high-purity, solid thin film. The primary advantage of this CVD approach is its superb conformality, allowing gaseous reactants to uniformly coat complex, high-aspect-ratio topographies like the pyramids on a textured silicon wafer. Among CVD, atomic layer deposition (ALD), has carved out a critical and immediate role in the fabrication of state-of-the-art PSTSCs.

Atomic layer deposition. ALD is a sophisticated variant of CVD that offers the ultimate level of precision by building films one atomic layer at a time. The process consists of sequential, self-limiting surface reactions as shown in Fig. 3i: a pulse of the first precursor gas is introduced to form a saturated monolayer on the substrate, followed by a purge with an inert gas to remove any unreacted molecules. A pulse of a second precursor gas is then introduced to react with the first layer, and a final purge completes the cycle.[95] This meticulous, layer-by-layer growth mechanism is perfectly suited for creating ultra-thin, pinhole-free, and perfectly conformal functional layers, which are critical for maximizing the performance and stability of monolithic PSTSCs.

From the first beginning, ALD was applied to deposited compact TiO_2 as an ETL directly on the n++/p++ tunnel junction, which enables bypassing the usage of a TCO recombination layer, achieving the first perovskite/silicon tandem efficiency of 13.7%.[96] Then, Bush *et al.* employed ALD-SnO_2 as a buffer layer underneath a sputtered ITO, thereby protecting the underlying functional layers from sputter damage and enabling integration of inverted PSTSC with a 23.6% efficiency.[97] After that, ALD has been extended to additional critical functional layers in PSTSCs. Recently, a $\sim$3–5 nm TiO_x grown by ALD served as an all-in one interconnect in PSTSCs, fulfilling the functions of silicon surface passivation, hole extraction from silicon, and recombination junction between perovskite top and silicon bottom cells, and then was capped

with a thin ALD-TiN_y layer, which demonstrated a 26.5% efficiency.[98] Fang *et al.* proposed a bilayer passivation structure with ALD-Al_2O_3/$PDAI_2$ to precisely modulate energy level alignment, reduce defect density, and suppress interfacial non-radiative recombination between perovskite/ETL interface by facilitating moderate n-type doping, and enhancing charge extraction and transport efficiency, which boosted a certified tandem efficiency up to 30.8%.[99] Moreover, an ALD copper-doping process is introduced to fabricate low-temperature NiO_x HTLs, tailored for textured PSTSCs, which leads to a 30.5% efficiency.[100] Collectively, these studies underscore the versatility of ALD in PSTSCs, highlighting its indispensable role in engineering atomically precise, stable, and high-performance perovskite/silicon tandem architectures.

Overall, vapor-phase deposition techniques have established themselves as indispensable part of the scalable fabrication of PSTSCs. Their solvent-free nature, superior uniformity, and excellent conformality over textured silicon substrates directly address the key manufacturing bottlenecks of solution-based deposition methods, which characterizes a powerful and versatile pathway toward highly stable, large-area monolithic PSTSCs.

2.3. Hybrid deposition of perovskite in large-area tandems

While solution-based and vapor-phase deposition methods each offer compelling advantages, each also carries inherent trade-offs when applied to large-area, monolithic PSTSCs. Solution-based methods offer tremendous compositional freedom such as solvents, additives and passivation layers, and high throughput, but struggle with conformal coating of large-area textured substrates and solvent-induced defects, non-uniformity and instability. Vapor-phase methods provide solvent-free, uniform and conformal coatings on fluctuated substrates and outstanding stability, but often limit compositional flexibility especially for organic compositions, and may require high vacuum/throughput equipment. In this light, hybrid deposition methods, which combine vapor and solution steps, emerge as a promising route that bridges the merits of both approaches.

Recently, studies have demonstrated the strong potential of hybrid deposition methods for scalable fabrication of large-area monolithic PSTSCs. Zheng *et al.* employed a hybrid deposition-thermal evaporation of inorganic precursors followed by blade coated organic solution to fabricate PSTSCs, highlighting solvent engineering as a key to up-scale in air and then achieving a 26.3% efficiency over an aperture area of 16 cm^2.[101] Er-Raji *et al.* combined evaporated PbI_2 with blade-coated organic halides, uncovering S-shaped coating dynamics in hybrid deposition which is different from the U-shaped curve in meniscus-guided coating as mentioned in Fig. 1b, and delivering $\sim$28% efficiency of their devices with high-quality perovskite layers (Fig. 4a).[102] By nucleation modification with sodium 2,5-difluorobenzoate to reduce nucleation energy barrier difference at various convex angles on evaporated inorganic layer, researchers fabricated compact, pinhole-free perovskite layers suited for tandem integration with slot-die coated organic salts, and then obtained a 28.28% efficiency over 19.9 cm^2 area.[103] With further optimization of a synergistic solvent and pre-treatment engineering by employing a mixed ethanol/isobutanol solvent in second slot-die coating procedure and near-infrared irradiation pre-heating in drying processes, the fully textured PSTSCs demonstrated an impressive efficiency of 27.14% for an aperture area of 110 cm^2 (Fig. 4b).[104] In addition, a recent study reported that inkjet printing is employed in the second step of a hybrid deposition strategy, where after an initial evaporation of inorganic materials, achieving an efficiency of 27.43% for the fully textured PSTSCs with conformal, homogeneous perovskite films up to the wafer's very edge (Fig. 4c).[105] Collectively, these studies establish hybrid deposition as a scalable and versatile strategy for high-performance PSTSCs, balancing conformality, compositional tunability, and manufacturability across increasingly large substrate areas.

In brief, hybrid deposition methods that merge vapor-phase and solution-based processing present a compelling pathway for scalable, high-performance perovskite absorber films, especially in the demanding architecture of monolithic PSTSCs. By capturing the advantages of conformal vapor scaffolding and flexible solution chemistry, they help surmount key challenges associated with textured substrates and large-area uniformity. At the same time, challenges persist: (1) the interdiffusion and reaction kinetics between the evaporated precursor and the solution salt must be carefully controlled to avoid unreacted scaffolds or residual compositions. (2) Scaling to large-area substrates still requires uniform meniscus control, blade speed optimization, and solvent drying management. With increasing reports of high efficiencies and growing understanding of process dynamics, hybrid deposition methods stand poised to accelerate the transition of PSTSCs from lab to fab.

A wide array of scalable deposition techniques has been explored for the fabrication of monolithic PSTSCs. Solution-based methods, vapor-phase approaches, and hybrid strategies have demonstrated varying degrees of success in producing uniform, high-quality perovskite films compatible with textured silicon bottom cells. Fig. 5 summarizes the progress in efficiency and stability for monolithic PSTSCs. Although spin-coated devices still yield the highest efficiency, this technique faces inherent scalability limitations (Fig. 5a). The pivotal advance lies in translating high performance into the sizes required for industrial applications. Currently, tandems on full-size M10 silicon wafers have achieved certified efficiencies up to 28.6%,[5] with breakthroughs on M6 wafers reaching 33.0% and 29.8% for rigid and flexible devices, respectively.[5,42] These milestones underscore the successful integration of scalable deposition techniques with commercial silicon photovoltaics.

However, concomitant with these efficiency achievements is a pronounced stability gap that now represents the primary barrier to commercialization (Fig. 5b). Maximum power point (MPP) tracking tests indicate that operational lifetimes for most high-efficiency tandems fall far short of the 25-year (based on 12 h operation per day) lifespan requirement for commercial modules. This challenge is exacerbated under real-world conditions. Outdoor testing shows that performance dropped to

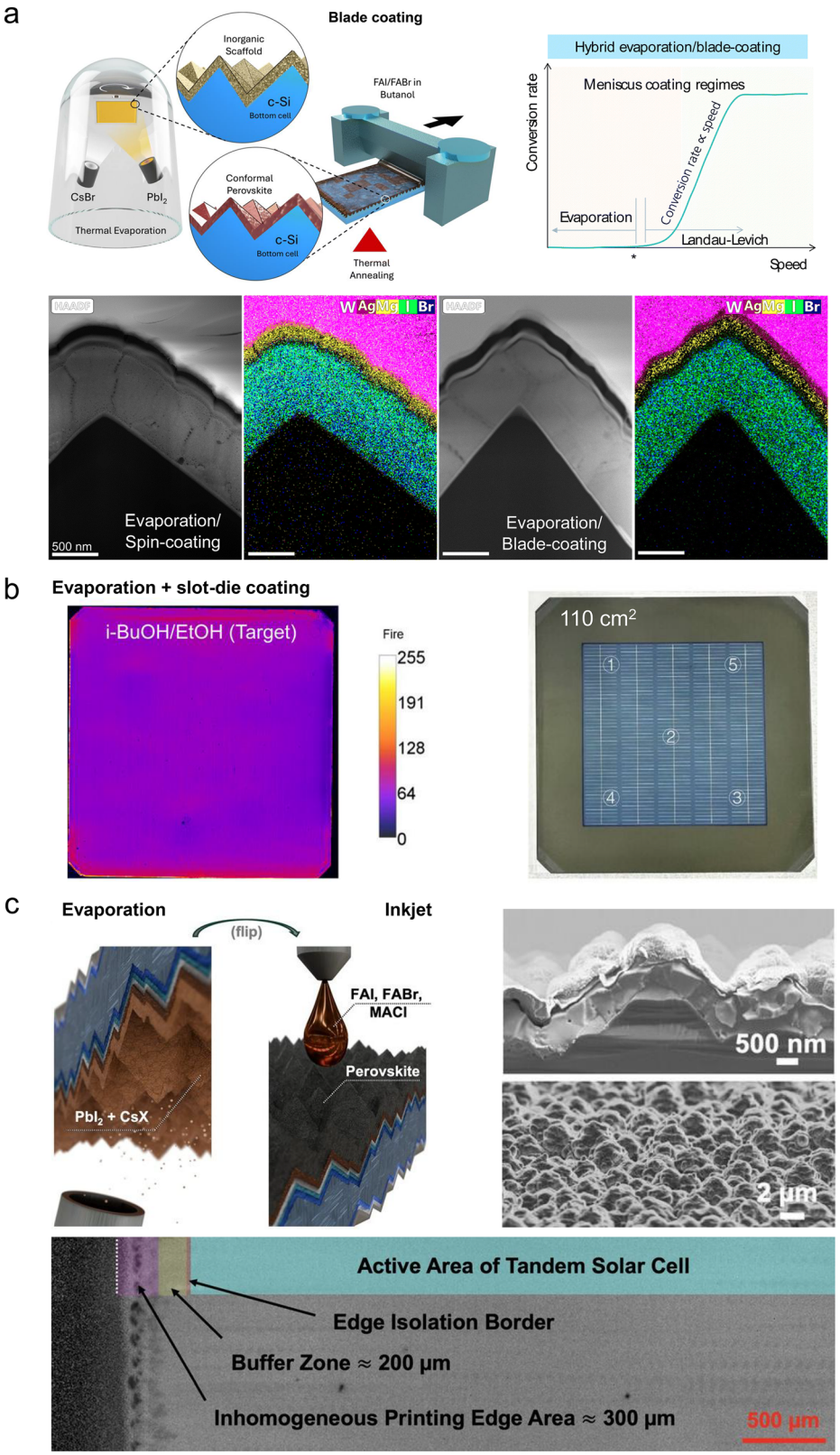

Fig. 4 Hybrid deposition methods for monolithic PSTSCs. (a) Schematic illustrating the hybrid evaporation/blade coating route for perovskite film, the meniscus coating regimes of the blade coating step in this route, STEM combined with energy-dispersive X-ray spectroscopy images of PSTSCs fabricated with hybrid evaporation/spin coating or evaporation/blade coating. Adapted from ref. 102 with permission from Royal Society of Chemistry,[102] copyright 2025. (b) The photoluminescence image of the hybrid deposited perovskite film on a M6 silicon wafer, the photograph of a representative tandem with a 110 cm^2 active area. Adapted from ref. 104 with permission from John Wiley and Sons,[104] copyright 2025. (c) Fabrication process schematic of PSTSCs using a hybrid evaporation/inkjet printing method, cross-section and surface SEM images of a fully textured PSTSC, k-map of the perovskite film on the outer millimeters of the substrate. Adapted from ref. 105 with permission from John Wiley and Sons,[105] copyright 2025.

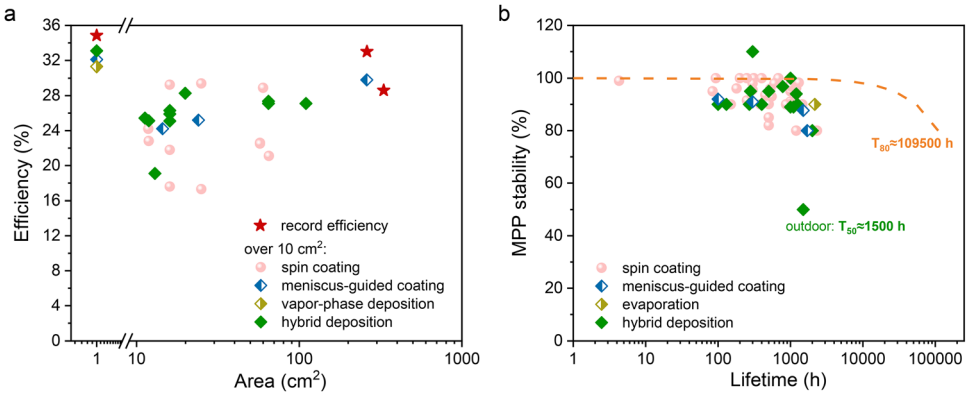

Fig. 5 Performance summary of monolithic PSTSCs with perovskite layers fabricated by different deposition methods. (a) Efficiencies of device area over 10 cm^2, record efficiencies from Martin A. Green Solar cell efficiency tables and the highest efficiency of each method within a 1 cm^2 aperture area. (b) MPP tracking stability. The lifespan curve of $T_{80} \approx 25$ year is calculated based on 12 hours of operation per day and a constant degradation rate.

about half of its initial efficiency within just 1500 hours, highlighting the severe impact of combined environmental stresses.[106] Many advances have been made to address the stability limitations, for example by developing scalable vapor-phase deposition method that produced highly stable PSTSCs on textured silicon wafers,[107] pointing toward viable pathways for commercial deployment. Nevertheless, achieving long-term outdoor stability and aligning perovskite lifetimes with the 25-year durability of commercial silicon panels remain critical barriers. Further work on scalable deposition processes, interfacial engineering, and encapsulation strategies will be essential to overcome these obstacles and realize the full potential of monolithic PSTSCs.

Table S1 provides an overview of above deposition methods, highlighting their working principles, kinetics control, silicon compatibility, film quality, implementation reliability, process complexity, cost, and industrial potential. In addition to perovskite deposition, techniques such as reaction-driven deposition, sputtering, ALD have proven essential for depositing functional layers including charge transport layers, interfacial layers, and electrodes, underscoring their significance in large-area device fabrication. We also present representative metrics reported in the literature to illustrate the industrial reliability of different scalable deposition techniques (Table S2). Collectively, these scalable deposition methods offer versatile availabilities for addressing the dual demands of high efficiency and large-scale manufacturability, paving the way toward the industrial realization of PSTSC technology.

3. Scalable drying methods and their advancements in PSTSCs

The deposition of high-quality films over large areas is a critical step in the manufacturing of monolithic PSTSCs. While coating techniques are widely recognized as fundamental, the drying process of them that follows is equally crucial, as it directly governs the crystallization kinetics, morphology, and ultimate optoelectronic properties of the layers. In large-area processing, achieving uniform drying across the entire substrate is particularly challenging. As the wet film transitions to a solid layer, the choice of drying method strongly influences the film morphology, coverage, defect density, and eventual device metrics. Fast, uniform, controlled drying is key to trigger homogeneous nucleation, suppress pin-holes or voids, control grain growth and crystallographic orientation of perovskite. This chapter systematically reviews the mechanisms and recent advances in scalable drying technologies, moving beyond traditional methods such as anti-solvent extraction and substrate preheating, to explore innovative approaches like spatially regulated gas flow, vacuum quench, and advanced radiative thermal management, examining recent progress and applicability to large-area and textured substrates, and discussing their advantages and limitations.

3.1. Anti-solvent extraction

During or after film coating, an anti-solvent is introduced *via* drip, bath or spray, which rapidly reduces the solubility of the perovskite precursor and thus triggers immediate supersaturation and nucleation, enabling fast crystallization and large-grain growth. The anti-solvent method controls film crystallization kinetics, which is widely used in the lab-fabrication of perovskite-based solar cells.

While conventional anti-solvent extraction in lab-scale spin coating typically relies on simple manual dripping, scalable fabrication demands more controlled and uniform solvent removal. As illustrated in Fig. 6a, several modified anti-solvent extraction strategies have been developed for large-area perovskite film formation, including multi-pipette dripping, dynamic dripping, anti-solvent bath, and anti-solvent spraying.[108–111] However, the implementation of such approaches in large-area monolithic PSTSCs remains scarce. Notably, Shi *et al.* employed an 8-channel pipetting gun to spin coat organic salt dissolved in ethanol *via* a sequential deposition strategy, and then achieving a 26.6% tandem efficiency over 64.64 cm^2 area.[112]

In short, this anti-solvent extraction method is highly effective at producing dense, pinhole-free films. However, despite the improved modes, it introduces a second solvent stream,

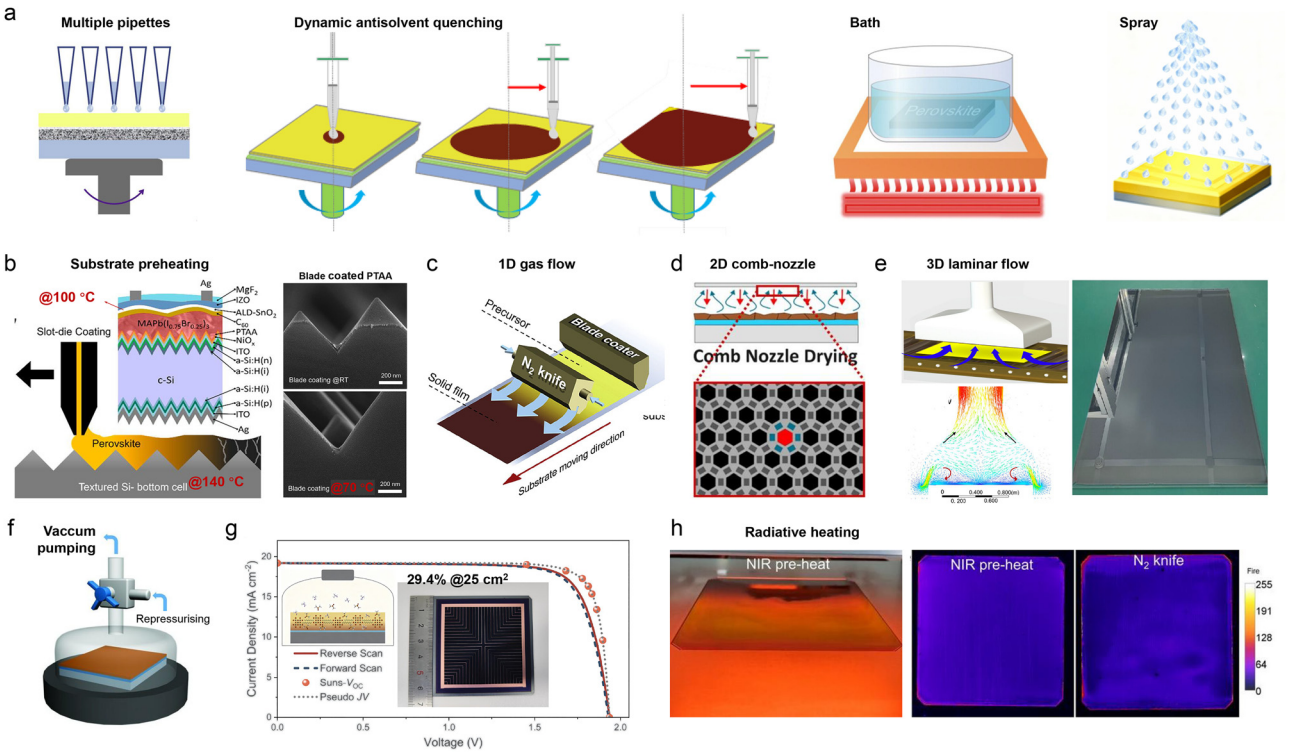

Fig. 6 Scalable drying methods. (a) Anti-solvent extraction drying methods for large-area drying, including multi-pipette dripping,[108] dynamic dripping,[109] anti-solvent bath[110] and anti-solvent spraying.[111] Adapted from ref. 108 with permission from Elsevier,[108] copyright 2020. Adapted from ref. 109 with permission from John Wiley and Sons,[109] copyright 2020. Adapted from ref. 110 with permission from The American Association for the Advancement of Science,[110] copyright 2021. Adapted from ref. 111 with permission from Royal Society of Chemistry,[111] copyright 2022. (b) Schematic and SEM images with pre-heated drying methods for the depositions of slot-die coated perovskite film, ALD-SnO_2 and blade coated PTAA.[31,39] Adapted from ref. 31 with permission from Elsevier,[31] copyright 2020. Adapted from ref. 39 with permission from American Chemical Society,[39] copyright 2020. Gas flow drying methods of (c) N_2 knife,[31] (d) 2D comb-nozzle[41] and (e) 3D laminar flow.[8] Adapted from ref. 31 with permission from Elsevier,[31] copyright 2020. Adapted from ref. 41 with permission from John Wiley and Sons,[41] copyright 2025. Adapted from ref. 8 with permission from The American Association for the Advancement of Science,[8] copyright 2025. (f) Schematic of vacuum quenching method. Adapted from ref. 115 with permission from The American Association for the Advancement of Science,[115] copyright 2016. (g) *J*–*V* curves and a photograph of a PSTSC with vacuum quenching dried perovskite film. Adapted from ref. 119 with permission from The American Association for the Advancement of Science,[119] copyright 2024. (h) NIR pre-heating a slot-die coated perovskite film, and photoluminescence images of perovskite films dried by NIR pre-heating and N_2 knife. Adapted from ref. 104 with permission from John Wiley and Sons,[104] copyright 2025.

increasing process complexity and chemical waste, which are important considerations for industrial-scale manufacturing.

3.2. Substrate preheating

The most fundamental approach to controlling solvent evaporation is substrate preheating. By heating the substrate to a specific temperature over room temperature before or during deposition, the rate of solvent evaporation is accelerated. This reduces the time available for undesirable solvent-precursor phase separation and can promote faster, more uniform nucleation of perovskite. The precise temperature provides a simple yet effective lever to tune the crystallization kinetics for a given solvent system.

To date, preheating technology has been applied to the deposition of ALD buffer layer, perovskite absorber layers, charge transport layers, and interface layers in monolithic PSTSCs (Fig. 6b and 2c),[31,39,50] demonstrating its great applicability. Thus, it is important to ensure the accuracy of the preheating temperature and its uniformity over a large area.

3.3. Gas flow

A directed high-velocity gas stream such as N_2, Ar and dry air, across the wet film accelerates solvent evaporation, increases supersaturation, triggers a high nucleation density, and thereby promotes more uniform crystal initiation rather than slow lateral growth. It can also assist in driving residual solvent away from films and reduce flow-driven inhomogeneity in the wet state.

The conventional gas knife employs a linear jet of high-pressure gas directed across the wet film surface, assisting solvent evaporation *via* enhanced convective mass transfer (Fig. 6c).[31] Many works on monolithic PSTSCs integrated in lab are implemented in this way.[16,31,32,113,114] However, because the airflow follows a 1D unidirectional pattern, a temporal delay arises between the leading and trailing edges of the substrate during large-area drying, which causes premature self-drying of the film near the trailing edge before the gas knife reaches it. A novel 2D comb-nozzle drying technique has been developed to enhance drying uniformity of large-area,

slot-die coated perovskite films (Fig. 6d), which employed a 20 × 20 cm^2 nozzle array composed of hexagon-shaped gas outlets surrounded by suction slits that locally remove drying air, enabling precise control of the heat and mass transfer coefficients across the substrate.[41] Moreover, Yan *et al.* developed a laminar air drying system using a 3D-printed airflow model to rapidly and uniformly dry square-meter-scale perovskite films (Fig. 6e). This laminar air dryer effectively overcomes key challenges in large-area perovskite film fabrication by emulating the uniform convective environment of spin coating while maintaining a stable, laminar airflow field. In addition, it demonstrates excellent compatibility with slot-die coated substrates up to 0.79 m^2, ensuring precise control over film thickness, solvent removal, and nucleation dynamics, which are crucial parameters for scalable, high-quality perovskite layer formation.[8] Therefore, various gas flow drying techniques have the potential to be a cornerstone technique for the scalable development of large-area monolithic PSTSCs.

3.4. Vacuum quenching

After coating the wet film, the substrate is transferred into a vacuum environment or subjected to rapid depressurization (Fig. 6f),[115] which lowers the solvent partial pressure, accelerates solvent evaporation, and induces rapid supersaturation, resulting in high nucleation density and film formation. However, this vacuum drying process typically produces a transient ''spike'' profile, where the convective air flow peaks within the first few milliseconds of pumping and decays to nearly zero after ~10 s.[8] Because this convective driving force is sustained only briefly, complete solvent removal can be challenging-particularly for systems containing high-boiling point solvents, potentially leading to incomplete drying or residual solvent retention.

Even so, there still are many works on monolithic PSTSCs with vacuum quenched perovskite layers. Wu *et al.* fabricated PSTSCs featuring mesoscopic perovskite top cells with vacuum quenched perovskite layers and high-temperature tolerant homojunction silicon bottom cells.[116] Xia *et al.* combined the vacuum quenching processing and interfacial passivation, integrating monolithic tandem structures with 24.01% efficiency.[117] With a tunneling oxide passivating contact silicon bottom cell produced on a production line, a 27.6% efficiency was achieved for a monolithic PSTSC with a vacuum flashed perovskite layer.[118] Last year, Chen *et al.* used oleylammonium iodide to stabilize the desired crystal nuclei and vacuum quenching to control surface tension, demonstrating a 29.4% efficiency for a PSTSC with a 25 cm^2 active area (Fig. 6g).[119] Although the engineering of high-throughput vacuum systems is a primary challenge, these results still indicate that vacuum quenching remains a good method for achieving superior film quality and device efficiencies.

3.5. Radiative heating

Radiative heating, particularly through near-infrared (NIR) irradiation, provides a non-contact and ultrafast annealing approach for film processing. By employing light in the 800–1500 nm wavelength range, which is efficiently absorbed by the substrate or the film itself, this technique enables rapid volumetric heating that accelerates solvent evaporation and promotes the growth of large, high-quality crystal grains. The entire process can be completed within a few seconds, markedly enhancing throughput and offering excellent compatibility with inline manufacturing.

Liu *et al.* employed a NIR preheating strategy to precisely regulate the solvent evaporation rate during perovskite film formation (Fig. 6h).[104] The absorbed NIR energy directly heated the wet perovskite layer through the solvent, enabling rapid solvent removal and controlled volatilization for enhanced large-area compositional uniformity. Luminescence characterization revealed excellent surface homogeneity across large-area films treated by NIR preheating. Remarkably, this approach yielded highly uniform perovskite films on M6-sized (166 × 166 mm^2) silicon bottom cells, and the resulting monolithic PSTSCs achieved an efficiency of 27.14% over a 110 cm^2 active area. Although the reports of NIR heating in monolithic PSTSCs remain limited, it shows great promise for enabling rapid, uniform, and scalable film processing.

In summary, drying methods are a critical element in the scalable deposition of large-area films, particularly for monolithic PSTSCs. The transition from wet films to solid layers requires careful control of solvent removal, supersaturation, nucleation and growth, as these factors influence crystallization behaviors in distinct ways. Different perovskite compositions exhibit varied crystallization dynamics due to differences in nucleation and phase evolution.[120] Mixed cation formulations such as FA/MA or FA/Cs, generally promote more uniform grain growth and reduced phase segregation compared with single-cation systems because the additional cations alter intermediate formation and stabilize the target α-phase, which in turn influences how films respond to drying conditions.[121] Therefore, it is essential to systematically screen and optimize drying protocols tailored to the specific perovskite compositions to ensure consistent nucleation, large grain formation, and homogeneous crystallization across large areas. Drying techniques each offer key advantages and trade-offs as shown in Table S3. For large-area, textured tandem fabrication, the drying step must not only be fast and uniform but also compatible with complex topographies, underlying silicon cells, and manufacturing-scale throughput. As this field moves toward industrial deployment, developing optimized, high-throughput, uniform drying methods tailored for large-area and textured substrates will be a major driver of yield, reliability and cost-effectiveness.

4. Outlook and future perspectives

The extensive research of scalable deposition and drying methods has been key to the progress of monolithic PSTSCs, propelling this photovoltaic technology from a realm of scientific possibility to one of tangible industrialization. As shown above, we now have a diverse, solid and evolved ''toolbox'' of

deposition and drying techniques. These tools have brought tandem efficiency close to 35%, a milestone achievement, and even higher. Currently, two main pathways are being widely explored: one is a ''performance-first'' route, which uses available methods to push for the highest possible efficiency and stability, and the other is a ''cost-first'' route that leans on solution processing like slot-die coating with inline drying, which appears promising for high-throughput and low-cost production. With the basic science now increasingly understood, the focus is clearly shifting from the lab toward the factory, where the main challenges are now manufacturing compatibility with minimal scaling-up performance losses.

4.1. Pathways towards mass production

As PSTSCs move closer to industrial realization, three key challenges are becoming increasingly prominent.

(1) Uniformity over large areas. Achieving large-area uniformity and maintaining a wide process window is the most urgent manufacturing hurdle. While fabricating a high-performance 1 cm^2 cell is a significant scientific achievement, replicating that performance with minimal efficiency deviation over industrial-scaled G12 wafers is an engineering challenge of a different magnitude. The process window as the range of parameters within which a high-quality film can be reliably produced, narrows dramatically with increasing area. In a process like slot-die coating, a delicate equilibrium exists between ink properties, substrate properties, coating parameters and the environmental conditions. On a large substrate, minor environmental fluctuations in temperature or humidity can disrupt this balance, leading to visible defects like stripes or ribs that are catastrophic for device performance.[17,122] The path forward, therefore, lies in engineering robustness into the process. This includes developing advanced ink formulations with additives that modulate rheology and crystallization kinetics, making the system more tolerant to process variations. Simultaneously, it requires the optimization of deposition and drying tools, such as designing more sophisticated slot-die heads and gas knives that deliver exceptionally stable fluid and gas flows over the entire coating areas.

(2) Long-term operational stability. Ensuring long-term operational stability remains the most critical barrier to widespread market adoption and bankability. The stability challenge for large-area monolithic PSTSCs is a systemic issue, extending beyond the intrinsic sensitivity of the perovskite material itself to be fundamentally intertwined with scalable fabrication processes, which introduce distinct problems that directly seed degradation pathways. Firstly, the rapid crystallization kinetics required for high-throughput deposition like in meniscus-guided coating often compromise microstructure. Fast solvent removal can hinder optimal crystal growth, resulting in films with smaller grains, a higher density of defective grain boundaries, and incorporated residual stress. This suboptimal microstructure inherently promotes ion migration, phase instability, and the accumulation of mechanical stress, triggering the degradation and then device instability.[123–125] Secondly, maintaining perfect uniformity across meter-scale areas is exceedingly difficult, leading to systematic macroscopic inhomogeneities.[8] Gradients in coating flow, drying rate, or thermal environment cause lateral variations in film thickness, composition, and residual stress.[104,126] These gradients establish localized weakest-link domains where degradation preferentially starts and propagates under operational stress, leading to non-uniform module aging which is negligible in more homogeneous lab-scale cells. Therefore, a comprehensive stability strategy must be co-designed with the manufacturing process and encompass the entire device stack. This means not only seeking stable absorber materials and charge transport layers but also engineering scalable processes to achieve controlled crystallization and superior uniformity. Integrating protective buffer layers *via* scalable methods such as ALD or spray coating, is crucial to shield functional layers from damage. Finally, robust encapsulation and edge-sealing are indispensable to defend against environmental invasion, preserving a device whose intrinsic stability has been maximized through prudent material and process design.

(3) Cost competitiveness. The overall cost structure must make sense. While the perovskite materials themselves are relatively cheap, the cumulative cost of other components and processes such as hole transport materials, indium-based transparent conductive electrodes, vacuum deposition systems, energy-intensive drying or annealing processes, remains significant. To make PSTSCs economically viable, research should focus on key levers: developing cheaper and more stable materials especially for charge transport layers, and streamlining manufacturing processes by using less material such as inkjet printing, increasing throughput like fast meniscus-guided coating, optimizing flash drying and annealing steps. This will help reduce the levelized cost of energy and make these tandems competitive with advanced silicon modules.

4.2. Paving the way for scalable manufacturing

Looking ahead, several research directions seem particularly important for tackling these challenges.

One crucial direction is the synergy and integration of different techniques to develop a hybrid mix-and-match manufacturing line to balance cost and performance. The future of PSTSC production is unlikely to be a single process but rather a modular system assembly of carefully screened, synergistic steps. We can envision a production line that leverages the strengths of multiple methods: a fast and low-cost meniscus-guided coater coats the perovskite layers; evaporators deposit charge transport layers; an ALD system applies ultra-thin passivation or buffer layers; a fast sputter grows the transparent conductive electrodes; and finally, a high-throughput screen printer deposits the top metal electrodes without requiring a vacuum. This modular approach would allow manufacturers to flexibly combine processes to optimize for their specific targets, whether it be maximum efficiency, lowest cost, or highest throughput. It is noteworthy that the layout of a production line must inherently consider the compatibility between the deposition techniques and the textured silicon bottom cell. Since the complete coverage of thin films on silicon pyramids is

influenced by a multitude of factors, such as the properties of the precursor ink, the surface characteristics of the substrates and the fluid dynamics of the deposition techniques,[31,127–131] it is not feasible to define a universal critical texture dimension. Therefore, texture design, such as size and aspect ratio of pyramid, must be co-optimized with the chosen techniques to prevent electrical shunts and minimize optical losses.

Subsequently, looking beyond conventional applications of stationary power generation, the advancement of high-efficiency flexible PSTSCs presents a compelling future direction.[42,132] Their unique attributes of high power-to-weight ratio and mechanical conformability could unlock transformative applications in sectors such as building-integrated photovoltaics, portable and wearable electronics, automotive integrated systems, and aerospace. The realization of this goal would naturally build upon the scalable deposition and drying methods discussed in this review, requiring their further adaptation to ensure compatibility with flexible substrates and long-term durability under mechanical stress. This direction aligns with the overarching themes of process integration, inspiring how the continuous evolution of scalable fabrication technologies can open new avenues for the entire field of PSTSCs.

Third, underpinning all efforts to improve yield and reliability is the need for robust *in situ* process monitoring and quality control. While complex artificial intelligence may be a long-term goal, the immediate, practical step is to integrate established process analytical technology into the production line. This involves integrating relatively simple and cost-effective sensors like optical cameras, spectrometers, and laser-based thickness gauges directly into the coating and drying equipment. These tools can provide real-time data on critical parameters like wet film thickness, drying-induced color changes which indicate crystallization states, and final film uniformity. This feedback can alert operators to process deviations or even trigger simple automated adjustments, forming the foundation of a quality control system that is essential for achieving the high yields required for mass production.

In conclusion, the journey of scalable deposition and drying methods has successfully elevated PSTSCs from a laboratory marvel to a technology poised for commercialization. The path forward is now not only about fundamental scientific discovery but also about dedicated engineering innovation. The success of this next stage will depend on the clever integration of existing techniques, a deep understanding and widening of the process window, and a systematic approach to optimizing stability and cost. Through this available and focused engineering effort, and with a belief to sustainable manufacturing, we have every reason to be confident that this remarkable photovoltaic technology will soon emerge as a mainstream, high-efficiency energy solution, ready to make a pivotal contribution to the global energy transition.

Conflicts of interest

The authors declare no conflict of interest.

Data availability

No primary research results, software or code have been included and no new data were generated or analysed as part of this review.

Acknowledgements

Y. H. acknowledges the support from Agency for Science, Technology and Research (A*STAR) under its MTC IRG Grant (M23M6c0108). C. K., C. L. and Y. H. are affiliated with the Solar Energy Research Institute of Singapore (SERIS), a research institute at the National University of Singapore. SERIS is supported by the National University of Singapore, the National Research Foundation Singapore, the Energy Market Authority of Singapore and the Singapore Economic Development Board.

References

1 National Renewable Energy Laboratory, Best Research-Cell Efficiency Chart, https://www.nrel.gov/pv/cell-efficiency (Access: October, 2025).
2 W. Shockley and H. J. Queisser, Detailed Balance Limit of Efficiency of p–n Junction Solar Cells, *J. Appl. Phys.*, 1961, **32**, 510–519.
3 S. Rühle, Tabulated values of the Shockley–Queisser limit for single junction solar cells, *Sol. Energy*, 2016, **130**, 139–147.
4 J. J. Cordell, M. Woodhouse and E. L. Warren, Technoeconomic analysis of perovskite/silicon tandem solar modules, *Joule*, 2025, **9**(2), 101781.
5 Martin A. Green, Ewan D. Dunlop, M. Yoshita, N. Kopidakis, K. Bothe, G. Siefer, X. Hao and Jessica Y. Jiang, Solar Cell Efficiency Tables (Version 66), *Prog. Photovoltaics Res. Appl.*, 2025, **33**, 795–810.
6 E. Aydin, T. G. Allen, M. De Bastiani, A. Razzaq, L. Xu, E. Ugur, J. Liu and S. De Wolf, Pathways toward commercial perovskite/silicon tandem photovoltaics, *Science*, 2024, **383**, eadh3849.
7 Oxford PV, 2024, https://www.oxfordpv.com/press-releases/oxford-pv-solar-technology-patent (accessed October, 2025).
8 B. Yan, W. Dai, Z. Wang, Z. Zhong, L. Zhang, M. Yu, Q. Zhou and Q. Ma, *et al.*, 3D laminar flow–assisted crystallization of perovskites for square meter–sized solar modules, *Science*, 2025, **388**, eadt5001.
9 A. Fell, M. Bivour, C. Messmer and M. Hermle, Is Shunt Quenching Relevant to Minimize Shunt Losses in Perovskite–Silicon Tandem Solar Cells?, *Solar RRL*, 2024, **8**, 2400571.
10 J. Zheng, C. F. J. Lau, H. Mehrvarz, F.-J. Ma, Y. Jiang, X. Deng, A. Soeriyadi and J. Kim, *et al.*, Large area efficient interface layer free monolithic perovskite/homo-junction-silicon tandem solar cell with over 20% efficiency, *Energy Environ. Sci.*, 2018, **11**, 2432–2443.
11 Au Rehman, E. P. Van Kerschaver, E. Aydin, W. Raja, T. G. Allen and S. De Wolf, Electrode metallization for

scaled perovskite/silicon tandem solar cells: Challenges and opportunities, *Prog. Photovoltaics Res. Appl.*, 2023, **31**, 429–442.

12 M. De Bastiani, G. Armaroli, R. Jalmood, L. Ferlauto, X. Li, R. Tao, G. T. Harrison and M. K. Eswaran, *et al.*, Mechanical Reliability of Fullerene/Tin Oxide Interfaces in Monolithic Perovskite/Silicon Tandem Cells, *ACS Energy Lett.*, 2022, **7**, 827–833.

13 E. Ugur, A. A. Said, P. Dally, S. Zhang, C. E. Petoukhoff, D. Rosas-Villalva, S. Zhumagali and B. K. Yildirim, *et al.*, Enhanced cation interaction in perovskites for efficient tandem solar cells with silicon, *Science*, 2024, **385**, 533–538.

14 L. Jia, S. Xia, J. Li, Y. Qin, B. Pei, L. Ding, J. Yin and T. Du, *et al.*, Efficient perovskite/silicon tandem with asymmetric self-assembly molecule, *Nature*, 2025, **644**, 912–919.

15 R. Yin, Y. Wu, Z. Huang, A. S. Vasenko, S. Xu and H. Zhou, Fabricating Perovskite Films for Solar Modules from Small to Large Scale, *Adv. Funct. Mater.*, 2025, **35**, 2419184.

16 A. S. Subbiah, S. Mannar, V. Hnapovskyi, A. R. Pininti, B. Vishal, L. V. Torres Merino, O. Matiash and O. Karalis, *et al.*, Efficient blade-coated perovskite/silicon tandems via interface engineering, *Joule*, 2025, **9**, 101767.

17 J. Li, J. Dagar, O. Shargaieva, O. Maus, M. Remec, Q. Emery, M. Khenkin and C. Ulbrich, *et al.*, Ink Design Enabling Slot-Die Coated Perovskite Solar Cells with >22% Power Conversion Efficiency, Micro-Modules, and 1 Year of Outdoor Performance Evaluation, *Adv. Energy Mater.*, 2023, **13**, 2203898.

18 W. Xu, Y. Yu, Y. Cui and J. Hou, Meniscus-guided coating for organic photovoltaic cells, *J. Mater. Chem. A*, 2025, **13**, 13657–13674.

19 M. Le Berre, Y. Chen and D. Baigl, From Convective Assembly to Landau−Levich Deposition of Multilayered Phospholipid Films of Controlled Thickness, *Langmuir*, 2009, **25**, 2554–2557.

20 Y. Deng, X. Zheng, Y. Bai, Q. Wang, J. Zhao and J. Huang, Surfactant-controlled ink drying enables high-speed deposition of perovskite films for efficient photovoltaic modules, *Nat. Energy*, 2018, **3**, 560–566.

21 X. Fanton and A. M. Cazabat, Spreading and Instabilities Induced by a Solutal Marangoni Effect, *Langmuir*, 1998, **14**, 2554–2561.

22 L. Landau and B. Levich, Dragging of a Liquid by a Moving Plate, ed. P. Pelcé, in *Dynamics of Curved Fronts*, Academic Press, San Diego, 1988, pp. 141–153.

23 Z. Zhang, A. Salamatin, F. Peng and K. G. Kornev, Dip coating of cylinders with Newtonian fluids, *J. Colloid Interface Sci.*, 2022, **607**, 502–513.

24 J.-W. Lee, D.-K. Lee, D.-N. Jeong and N.-G. Park, Control of Crystal Growth toward Scalable Fabrication of Perovskite Solar Cells, *Adv. Funct. Mater.*, 2019, **29**, 1807047.

25 Y.-H. Seo, S.-P. Cho, H.-J. Lee, Y.-J. Kang, S.-N. Kwon and S.-I. Na, Temperature-controlled slot-die coating for efficient and stable perovskite solar cells, *J. Power Sources*, 2022, **539**, 231621.

26 C. Huang, S. Tan, B. Yu, Y. Li, J. Shi, H. Wu, Y. Luo and D. Li, *et al.*, Meniscus-modulated blade coating enables high-quality α-phase formamidinium lead triiodide crystals and efficient perovskite minimodules, *Joule*, 2024, **8**, 2539–2553.

27 Y. Xu, G. J. Dixon, Q. Xie, J. F. Gilchrist, B. M. Cossairt, D. S. Ginger and E. Reichmanis, Landau–Levich Scaling for Optimization of Quantum Dot Layer Morphology and Thickness in Quantum-Dot Light-Emitting Diodes, *ACS Nano*, 2025, **19**, 5680–5687.

28 K. Sun, Z. Wang, N. Li, L. Liu, W. Xiong, Z. Xu, Z. Geng and X. Guo, *et al.*, Dynamic Reconstruction of Fluid Interface Manipulated by Fluid Balancing Agent for Scalable Efficient Perovskite Solar Cells, *Adv. Mater.*, 2025, **37**, 2419419.

29 Z. Qiang, Y. Wu, X. Gao, Y. Gong, Y. Liu, X. Zhao, H. Tian and W. Wang, *et al.*, A scalable method for fabricating monolithic perovskite/silicon tandem solar cells based on low-cost industrial silicon bottom cells, *Chem. Eng. J.*, 2024, **495**, 153422.

30 S. Siegrist, P. Nandi, R. K. Kothandaraman, A. Abdessalem, A. N. Tiwari and F. Fu, Understanding Coating Thickness and Uniformity of Blade-Coated SnO2 Electron Transport Layer for Scalable Perovskite Solar Cells, *Solar RRL*, 2023, **7**, 2300273.

31 B. Chen, Z. J. Yu, S. Manzoor, S. Wang, W. Weigand, Z. Yu, G. Yang and Z. Ni, *et al.*, Blade-Coated Perovskites on Textured Silicon for 26%-Efficient Monolithic Perovskite/Silicon Tandem Solar Cells, *Joule*, 2020, **4**, 850–864.

32 A. S. Subbiah, L. V. Torres Merino, A. R. Pininti, V. Hnapovskyi, S. Mannar, E. Aydin, A. Razzaq and T. G. Allen, *et al.*, Enhancing the Performance of Blade-Coated Perovskite/Silicon Tandems via Molecular Doping and Interfacial Energy Alignment, *ACS Energy Lett.*, 2024, **9**, 727–731.

33 D. Pu, S. Zhou, H. Guan, P. Jia, G. Chen, H. Fang, S. Fu and C. Wang, *et al.*, Enhancing Efficiency and Intrinsic Stability of Large-Area Blade-Coated Wide-Bandgap Perovskite Solar Cells Through Strain Release, *Adv. Funct. Mater.*, 2024, **34**, 2314349.

34 D.-N. Jeong, D.-K. Lee, S. Seo, S. Y. Lim, Y. Zhang, H. Shin, H. Cheong and N.-G. Park, Perovskite Cluster-Containing Solution for Scalable D-Bar Coating toward High-Throughput Perovskite Solar Cells, *ACS Energy Lett.*, 2019, **4**, 1189–1195.

35 J. W. Yoo, J. Jang, U. Kim, Y. Lee, S.-G. Ji, E. Noh, S. Hong and M. Choi, *et al.*, Efficient perovskite solar mini-modules fabricated via bar-coating using 2-methoxyethanol-based formamidinium lead tri-iodide precursor solution, *Joule*, 2021, **5**, 2420–2436.

36 R. Shimono, R. Nishikubo, M. Pylnev, F. Ishiwari, A. Wakamiya and A. Saeki, Bar Coating Process of Two-Dimensional Lead Iodide Perovskite Solar Cells: Effects of Vertical Orientation, Anisotropic Photoconductivity, and Conversion Time, *ACS Appl. Energy Mater.*, 2023, **6**, 9381–9389.

37 S. Mandati, R. Dileep, G. Veerappan and E. Ramasamy, Large area bar coated TiO2 electron transport layers for perovskite solar cells with excellent performance homogeneity, *Sol. Energy*, 2022, **240**, 258–268.
38 Y. Tu, J. Ye, G. Yang, Y. Zang, L. Zhang, Y. Wang, G. Li and L. Chu, *et al.*, Slot-die coating fabrication of perovskite solar cells toward commercialization, *J. Alloys Compd.*, 2023, **942**, 169104.
39 A. S. Subbiah, F. H. Isikgor, C. T. Howells, M. De Bastiani, J. Liu, E. Aydin, F. Furlan and T. G. Allen, *et al.*, High-Performance Perovskite Single-Junction and Textured Perovskite/Silicon Tandem Solar Cells via Slot-Die-Coating, *ACS Energy Lett.*, 2020, **5**, 3034–3040.
40 K. Xu, A. Al-Ashouri, Z.-W. Peng, E. Köhnen, H. Hempel, F. Akhundova, J. A. Marquez and P. Tockhorn, *et al.*, Slot-Die Coated Triple-Halide Perovskites for Efficient and Scalable Perovskite/Silicon Tandem Solar Cells, *ACS Energy Lett.*, 2022, **7**, 3600–3611.
41 K. Geistert, R. Pappenberger, P. Scharfer, P. Cavadini, W. Schabel, F. Sadegh, D. B. Ritzer and B. Abdollahi Nejand, *et al.*, Spatially Regulated Gas Flow Control for Batch-Drying of Large Area Slot-Die-Coated Perovskite Thin Films, *Adv. Energy Mater.*, 2025, **15**, 2500923.
42 Z. Fang, L. Ding, Y. Yang, X. Gu, H. Li, H. Chen, Y. Yin and W. Wang, *et al.*, Flexible perovskite/silicon tandem solar cell with a dual-buffer layer, *Nature*, 2026, **649**, 65–72.
43 M. Yang, Z. Li, M. O. Reese, O. G. Reid, D. H. Kim, S. Siol, T. R. Klein and Y. Yan, *et al.*, Perovskite ink with wide processing window for scalable high-efficiency solar cells, *Nat. Energy*, 2017, **2**, 17038.
44 T. Bu, J. Li, H. Li, C. Tian, J. Su, G. Tong, L. K. Ono and C. Wang, *et al.*, Lead halide–templated crystallization of methylamine-free perovskite for efficient photovoltaic modules, *Science*, 2021, **372**, 1327–1332.
45 J. Li, C. Jin, R. Jiang, J. Su, T. Tian, C. Yin, J. Meng and Z. Kou, *et al.*, Homogeneous coverage of the low-dimensional perovskite passivation layer for formamidinium–caesium perovskite solar modules, *Nat. Energy*, 2024, **9**, 1540–1550.
46 C. Wang, Y. Mo, X. Gao, Q. Huang, T. Bu, Q. Li, Y.-B. Cheng and F. Huang, SnO_2 ink engineering for printing efficient flexible perovskite solar modules, *Sci. Adv.*, 2025, **11**, eadu1116.
47 B. Kang and F. Yan, Emerging strategies for the large-scale fabrication of perovskite solar modules: from design to process, *Energy Environ. Sci.*, 2025, **18**, 3917–3954.
48 A. T. Barrows, A. J. Pearson, C. K. Kwak, A. D. F. Dunbar, A. R. Buckley and D. G. Lidzey, Efficient planar heterojunction mixed-halide perovskite solar cells deposited via spray-deposition, *Energy Environ. Sci.*, 2014, **7**, 2944–2950.
49 J. Chen, S. Yang, L. Jiang, K. Fan, Z. Liu, W. Liu, W. Li and H. Huang, *et al.*, Surface Molecular Engineering for Fully Textured Perovskite/Silicon Tandem Solar Cells, *Angew. Chem., Int. Ed.*, 2024, **63**, e202407151.
50 N. Liu, G. Zhang, M. Wei, L. Yang, H. Gu, L. Zeng, X. Zhang and Y. Geng, *et al.*, Particle decoration enables solution-processed perovskite integration with fully-textured silicon for efficient tandem solar cells, *Nat. Commun.*, 2025, **16**, 9435.
51 J. H. Heo, F. Zhang, C. Xiao, S. J. Heo, J. K. Park, J. J. Berry, K. Zhu and S. H. Im, Efficient and Stable Graded $CsPbI_{3-x}Br_x$ Perovskite Solar Cells and Submodules by Orthogonal Processable Spray Coating, *Joule*, 2021, **5**, 481–494.
52 H. Huang, J. Shi, L. Zhu, D. Li, Y. Luo and Q. Meng, Two-step ultrasonic spray deposition of CH3NH3PbI3 for efficient and large-area perovskite solar cell, *Nano Energy*, 2016, **27**, 352–358.
53 Y. Jiang, C. Wu, L. Li, K. Wang, Z. Tao, F. Gao, W. Cheng and J. Cheng, *et al.*, All electrospray printed perovskite solar cells, *Nano Energy*, 2018, **53**, 440–448.
54 T. Cao, Z. Yang, H. Zhang and Y. Wang, Inkjet printing quality improvement research progress: A review, *Heliyon*, 2024, **10**, e30163.
55 L. Tan, H. Jiang, R. Yang, L. Shen, C. Sun, Y. Jin, X. Guan and P. Song, *et al.*, Quantitative Surface Passivation Through Drop-on-Demand Inkjet Printing Enables Highly Efficient Perovskite Solar Cells, *Adv. Energy Mater.*, 2024, **14**, 2400549.
56 Z. Du, L. Zhang, Y. Du, X. Wei, X. Du, X. Lin, J. Liu and Y. Huang, *et al.*, Controlling the Polymer Ink's Rheological Properties to Form Single and Stable Droplet, *Coatings*, 2024, **14**, 600.
57 Y. Liu and B. Derby, Experimental study of the parameters for stable drop-on-demand inkjet performance, *Phys. Fluids*, 2019, **31**, 032004.
58 N. Reis and B. Derby, Ink Jet Deposition of Ceramic Suspensions: Modeling and Experiments of Droplet Formation, *MRS Online Proc. Libr.*, 2000, **625**, 117.
59 R. Pesch, A. Diercks, J. Petry, A. Welle, R. Pappenberger, F. Schackmar, H. Eggers and J. Sutter, *et al.*, Hybrid Two-Step Inkjet-Printed Perovskite Solar Cells, *Solar RRL*, 2024, **8**, 2400165.
60 TAIYANGNEWS, China Solar PV News Snippets-Phenosolar's R&D Inkjet Tandem Cell Line Online & More, 2025, https://taiyangnews.info/.
61 A. Verma, D. Martineau, S. Abdolhosseinzadeh, J. Heier and F. Nüesch, Inkjet printed mesoscopic perovskite solar cells with custom design capability, *Mater. Adv.*, 2020, **1**, 153–160.
62 D. Lu, M. Jamshidi, C. Dun, J. J. Urban, J. M. Gardner and L. Belova, Inkjet-printed Ce-doped SnOx electron transport layer for improved performance of planar perovskite solar cells, *Mater. Adv.*, 2024, **5**, 6270–6276.
63 V. V. Satale, S. Chowdhury, A. Mohamed, D.-H. Kim, S. Cho, J.-S. Lee and J.-W. Kang, Green Solvent Enabled Perovskite Ink for Ambient-Air-Processed Efficient Inkjet-Printed Perovskite Solar Cells, *Adv. Funct. Mater.*, 2025, **35**, 2503717.
64 C. Chen, J. Chen, H. Han, L. Chao, J. Hu, T. Niu, H. Dong and S. Yang, *et al.*, Perovskite solar cells based on screen-printed thin films, *Nature*, 2022, **612**, 266–271.

65 N. Zavanelli, J. Kim and W.-H. Yeo, Recent Advances in High-Throughput Nanomaterial Manufacturing for Hybrid Flexible Bioelectronics, *Materials*, 2021, **14**, 2973.
66 C. Chen, C. Ran, C. Guo, Q. Yao, J. Wang, T. Niu, D. Li and L. Chao, *et al.*, Fully Screen-Printed Perovskite Solar Cells with 17% Efficiency via Tailoring Confined Perovskite Crystallization within Mesoporous Layer, *Adv. Energy Mater.*, 2023, **13**, 2302654.
67 M. Duan, J. Yang, T. Li, J. Wen, B. Ren, K. Wang, Y. Xia and H. Zhang, *et al.*, Mechanically stable screen-printed flexible perovskite solar cells via selective self-assembled siloxane coupling agents, *npj Flexible Electron.*, 2025, **9**, 30.
68 B. A. Kamino, B. Paviet-Salomon, S.-J. Moon, N. Badel, J. Levrat, G. Christmann, A. Walter and A. Faes, *et al.*, Low-Temperature Screen-Printed Metallization for the Scale-Up of Two-Terminal Perovskite–Silicon Tandems, *ACS Appl. Energy Mater.*, 2019, **2**, 3815–3821.
69 A. De Rose, D. Erath, V. Nikitina, J. Schube, D. Güldali, Ä. Minat, T. Rößler and A. Richter, *et al.*, Low-temperature metallization & interconnection for silicon heterojunction and perovskite silicon tandem solar cells, *Sol. Energy Mater. Sol. Cells*, 2023, **261**, 112515.
70 Y. Y. Kim, T.-Y. Yang, R. Suhonen, M. Välimäki, T. Maaninen, A. Kemppainen, N. J. Jeon and J. Seo, Gravure-Printed Flexible Perovskite Solar Cells: Toward Roll-to-Roll Manufacturing, *Adv. Sci.*, 2019, **6**, 1802094.
71 Y. Y. Kim, T.-Y. Yang, R. Suhonen, A. Kemppainen, K. Hwang, N. J. Jeon and J. Seo, Roll-to-roll gravure-printed flexible perovskite solar cells using eco-friendly antisolvent bathing with wide processing window, *Nat. Commun.*, 2020, **11**, 5146.
72 F. Bisconti, A. Giuri, R. Suhonen, T. M. Kraft, M. Ylikunnari, V. Holappa, R. Po and P. Biagini, *et al.*, One-step polymer assisted roll-to-roll gravure-printed perovskite solar cells without using anti-solvent bathing, *Cell Rep. Phys. Sci.*, 2021, **2**, 100639.
73 Y. Zhang, S.-G. Kim, D. Lee, H. Shin and N.-G. Park, Bifacial stamping for high efficiency perovskite solar cells, *Energy Environ. Sci.*, 2019, **12**, 308–321.
74 J. Lee, G. Jang, S. Ma, C. U. Lee, J. Son, W. Jeong and J. Moon, Universal Bifacial Stamping Approach Enabling Reverse-Graded Ruddlesden-Popper 2D Perovskite Solar Cells, *Small*, 2022, **18**, 2202159.
75 A. Kessel, J. Moon, J. F. Benitez-Rodriguez, H. Deng, W. Mao, T. Alan, U. Bach and J. Jasieniak, Patterning of Hybrid Metal Halide Perovskite via Printed Molecular Templates, *Adv. Mater. Technol.*, 2024, **9**, 2302043.
76 J. Hyun, K. M. Yeom, H. E. Lee, D. Kim, H.-S. Lee, J. H. Noh and Y. Kang, Efficient n-i-p Monolithic Perovskite/Silicon Tandem Solar Cells with Tin Oxide via a Chemical Bath Deposition Method, *Energies*, 2021, **14**, 7614.
77 Y. Xiang, T. Yu, D. Xue, C. Zhu, Z. Chen, K. Ren, C. Li and H. Zhang, *et al.*, Electrodeposition Preparation of Perovskite Solar Cells with an Efficiency Exceeding 19%, *Small*, 2025, **21**, 2502302.
78 D. Aji and P. Pakawatpanurut, Li-Doped SnO2 Electron Transport Layer for High-Performance Perovskite Solar Cell Fabricated Using Magnetic Field-Assisted Electrodeposition, *Key Eng. Mater.*, 2022, **927**, 161–166.
79 H. Chen, Z. Wei, X. Zheng and S. Yang, A scalable electrodeposition route to the low-cost, versatile and controllable fabrication of perovskite solar cells, *Nano Energy*, 2015, **15**, 216–226.
80 J. Han, K. Park, S. Tan, Y. Vaynzof, J. Xue, E. W.-G. Diau, M. G. Bawendi and J.-W. Lee, *et al.*, Perovskite solar cells, *Nat. Rev. Methods Primers*, 2025, **5**, 3.
81 M. Roß, S. Severin, M. B. Stutz, P. Wagner, H. Köbler, M. Favin-Lévêque, A. Al-Ashouri and P. Korb, *et al.*, Co-Evaporated Formamidinium Lead Iodide Based Perovskites with 1000 h Constant Stability for Fully Textured Monolithic Perovskite/Silicon Tandem Solar Cells, *Adv. Energy Mater.*, 2021, **11**, 2101460.
82 S. Chozas-Barrientos, A. Paliwal, F. Ventosinos, C. Roldán-Carmona, L. Gil-Escrig, V. Held, P. Carroy and D. Muñoz, *et al.*, Molecular Recombination Junction for Vacuum-Deposited Perovskite/Silicon Two-Terminal Tandem Solar Cells, *ACS Energy Lett.*, 2025, **10**, 1733–1740.
83 Z. Dong, J. Hu, X. Guo, Z. Shi, H. Chen, Y. Wang, R. Luo and J. A. Steele, *et al.*, Intermediate phase evolution for stable and oriented evaporated wide-bandgap perovskite solar cells, *Nat. Mater.*, 2025, DOI: 10.1038/s41563-025-02375-8.
84 Y. Xu, K. Xu, T. Pan, X. Ke, Y. Li, N. Meng, X. Shi and J. Liu, *et al.*, Fully thermally evaporated perovskite solar cells based on reverse layer-by-layer deposition, *Nat. Photonics*, 2025, **19**, 1345–1352.
85 N. Rodkey, I. Gomar-Fernández, F. Ventosinos, C. Roldan-Carmona, L. J. A. Koster and H. J. Bolink, Close-Space Sublimation as a Scalable Method for Perovskite Solar Cells, *ACS Energy Lett.*, 2024, **9**, 927–933.
86 C. Wang, Y. Zhao, T. Ma, Y. An, R. He, J. Zhu, C. Chen and S. Ren, *et al.*, A universal close-space annealing strategy towards high-quality perovskite absorbers enabling efficient all-perovskite tandem solar cells, *Nat. Energy*, 2022, **7**, 744–753.
87 G. Li, J. Y. L. Ho, M. Wong and H.-S. Kwok, Low cost, high throughput and centimeter-scale fabrication of efficient hybrid perovskite solar cells by closed space vapor transport, *Phys. Status Solidi RRL*, 2016, **10**, 153–157.
88 T. Abzieher, C. P. Muzzillo, M. Mirzokarimov, G. Lahti, W. F. Kau, D. M. Kroupa, S. G. Cira and H. W. Hillhouse, *et al.*, Continuous flash sublimation of inorganic halide perovskites: overcoming rate and continuity limitations of vapor deposition, *J. Mater. Chem. A*, 2024, **12**, 8405–8419.
89 M. Bellardita, A. Di Paola, S. Yurdakal and L. Palmisano, Preparation of Catalysts and Photocatalysts Used for Similar Processes, ed. G. Marcì, L. Palmisano, *Heterogeneous Photocatalysis*, Elsevier, 2019, ch. 2, pp. 25–56.
90 A. Baptista, F. Silva, J. Porteiro, J. Míguez and G. Pinto, Sputtering Physical Vapour Deposition (PVD) Coatings: A Critical Review on Process Improvement and Market Trend Demands, *Coatings*, 2018, **8**, 402.

91 Y. Hou, E. Aydin, M. De Bastiani, C. Xiao, F. H. Isikgor, D.-J. Xue, B. Chen and H. Chen, *et al.*, Efficient tandem solar cells with solution-processed perovskite on textured crystalline silicon, *Science*, 2020, **367**, 1135–1140.

92 E. Aydin, J. Liu, E. Ugur, R. Azmi, G. T. Harrison, Y. Hou, B. Chen and S. Zhumagali, *et al.*, Ligand-bridged charge extraction and enhanced quantum efficiency enable efficient n–i–p perovskite/silicon tandem solar cells, *Energy Environ. Sci.*, 2021, **14**, 4377–4390.

93 J. M. Cd Silva Filho, V. A. Ermakov and F. C. Marques, Perovskite Thin Film Synthesised from Sputtered Lead Sulphide, *Sci. Rep.*, 2018, **8**, 1563.

94 J.-K. Hwang, S.-W. Lee, W. Lee, S. Bae, D. Kang, S.-H. Jeong, S. Lee and D. Pyun, *et al.*, Sputtered PbI_2 with Post-Processing for Perovskite Solar Cells, *Solar RRL*, 2023, **7**, 2300214.

95 E. Kessels, A. Devi, J.-S. Park, M. Ritala, A. Yanguas-Gil and C. Wiemer, Atomic layer deposition, *Nat. Rev. Methods Primers*, 2025, **5**, 66.

96 J. P. Mailoa, C. D. Bailie, E. C. Johlin, E. T. Hoke, A. J. Akey, W. H. Nguyen, M. D. McGehee and T. Buonassisi, A 2-terminal perovskite/silicon multijunction solar cell enabled by a silicon tunnel junction, *Appl. Phys. Lett.*, 2015, **106**, 121105.

97 K. A. Bush, A. F. Palmstrom, Z. J. Yu, M. Boccard, R. Cheacharoen, J. P. Mailoa, D. P. McMeekin and R. L. Z. Hoye, *et al.*, 23.6%-efficient monolithic perovskite/silicon tandem solar cells with improved stability, *Nat. Energy*, 2017, **2**, 17009.

98 T. Matsui, C. McDonald, A. Mirzehmet, J. McQueen, R. S. Bonilla and H. Sai, Monolithic Perovskite/Silicon Tandem Solar Cells Enabled by Multifunctional TiOx Interconnects, *Small*, 2025, **21**, 2500969.

99 L. Fang, M. Ren, B. Li, X. Liu, S. Liang, J. Petermann, M. Gholipoor and T. Zhao, *et al.*, Interfacial design strategies for stable and high-performance perovskite/silicon tandem solar cells on industrial silicon cells, *Nat. Commun.*, 2025, **16**, 8881.

100 Z. Zhu, S. Yuan, K. Mao, H. Meng, F. Cai, T. Li, X. Feng and H. Guo, *et al.*, Low-Temperature Atomic Layer Deposition of Hole Transport Layers for Enhanced Performance and Scalability in Textured Perovskite/Silicon Tandem Solar Cells, *Adv. Energy Mater.*, 2024, **14**, 2402365.

101 X. Zheng, W. Kong, J. Wen, J. Hong, H. Luo, R. Xia, Z. Huang and X. Luo, *et al.*, Solvent engineering for scalable fabrication of perovskite/silicon tandem solar cells in air, *Nat. Commun.*, 2024, **15**, 4907.

102 O. Er-raji, A. A. Said, A. S. Subbiah, V. Hnapovskyi, B. Vishal, A. R. Pininti, M. Marengo and M. Bivour, *et al.*, Coating dynamics in two-step hybrid evaporated/blade-coated perovskites for scalable fully-textured perovskite/silicon tandem solar cells, *EES Solar*, 2025, **1**, 419–430.

103 H. Li, Z. Zhang, Y. Wei, B. An, J. Liao, X. Lv, W. Lv and J. Yang, *et al.*, Nucleation Modification in Two-Step Slot-Die Coating Toward Efficient Large Scale Perovskite/Silicon Tandems Based on Commercial Silicon Cells, *Adv. Mater.*, 2025, **37**, 2501961.

104 Z. Liu, S. Yang, Y. Tian, L. Jiang, G. Li, J. Yao, M. Liu and Z. Xiong, *et al.*, Homogeneity Regulation in Sequential Fabricated Perovskite Film for Industrial-Scale Deposition of Fully-Textured Perovskite/Silicon Tandem Cells, *Adv. Mater.*, 2025, e11177, DOI: 10.1002/adma.202511177.

105 R. Pesch, J. Petry, J. Petermann, R. Pappenberger, T. Kuechle, J. Schenck, L. P. Rothbauer and L. Fang, *et al.*, Efficient Perovskite/Silicon Tandem Solar Cells Using Hybrid Two-Step Inkjet Printing with Edge Isolation Precision, *Small Sci.*, 2025, **5**, e202500362.

106 O. Er-raji, C. Messmer, R. R. Pradhan, O. Fischer, V. Hnapovskyi, S. Kosar, M. Marengo and M. List, *et al.*, Electron accumulation across the perovskite layer enhances tandem solar cells with textured silicon, *Science*, 2025, **390**, eadx1745.

107 N. Li, X. Niu, Z. Dong, J. Hu, R. Luo, S. Yang, Q. Zhou and Z. Shi, *et al.*, Optimal perovskite vapor partitioning on textured silicon for high-stability tandem solar cells, *Science*, 2025, **390**, eadz3698.

108 C. Wang, G. Tan, X. Luo, J. Li, X. Gao, Y. Mo, X.-L. Zhang and X. Wang, *et al.*, How to fabricate efficient perovskite solar mini-modules in lab, *J. Power Sources*, 2020, **466**, 228321.

109 T. Bu, X. Liu, J. Li, W. Huang, Z. Wu, F. Huang, Y.-B. Cheng and J. Zhong, Dynamic Antisolvent Engineering for Spin Coating of $10 \times 10\,cm^2$ Perovskite Solar Module Approaching 18%, *Solar RRL*, 2020, **4**, 1900263.

110 N. Li, X. Niu, L. Li, H. Wang, Z. Huang, Y. Zhang, Y. Chen and X. Zhang, *et al.*, Liquid medium annealing for fabricating durable perovskite solar cells with improved reproducibility, *Science*, 2021, **373**, 561–567.

111 O. Telschow, M. Albaladejo-Siguan, L. Merten, A. D. Taylor, K. P. Goetz, T. Schramm, O. V. Konovalov and M. Jankowski, *et al.*, Preserving the stoichiometry of triple-cation perovskites by carrier-gas-free antisolvent spraying, *J. Mater. Chem. A*, 2022, **10**, 19743–19749.

112 B. Shi, P. Liu, Z. Sunli, W. Han, C. Sun, Y. Liu, Y. Luo and J. Si, *et al.*, Halogen anion pre-homogenization of sequentially deposited wide bandgap perovskites for commercial textured perovskite/silicon tandem solar cells, *Energy Environ. Sci.*, 2025, **18**, 6297–6306.

113 X. Ge, Z. Huang, B. Shi, P. Wang, Z. Liu, Y. Gao, X. Du and Y. Zhao, *et al.*, Crystallization Control of Blade-Coated Wide Bandgap FACs-Based Perovskite, *Adv. Funct. Mater.*, 2025, **35**, 2417493.

114 C. Duan, H. Gao, K. Xiao, V. Yeddu, B. Wang, R. Lin, H. Sun and P. Wu, *et al.*, Scalable fabrication of wide-bandgap perovskites using green solvents for tandem solar cells, *Nat. Energy*, 2025, **10**, 318–328.

115 X. Li, D. Bi, C. Yi, J.-D. Décoppet, J. Luo, S. M. Zakeeruddin, A. Hagfeldt and M. Grätzel, A vacuum flash–assisted solution process for high-efficiency large-area perovskite solar cells, *Science*, 2016, **353**, 58–62.

116 Y. Wu, D. Yan, J. Peng, T. Duong, Y. Wan, S. P. Phang, H. Shen and N. Wu, *et al.*, Monolithic perovskite/silicon-homojunction tandem solar cell with over 22% efficiency, *Energy Environ. Sci.*, 2017, **10**, 2472–2479.

117 R. Xia, Y. Xu, B. Chen, H. Kanda, M. Franckevičius, R. Gegevičius, S. Wang and Y. Chen, *et al.*, Interfacial passivation of wide-bandgap perovskite solar cells and tandem solar cells, *J. Mater. Chem. A*, 2021, **9**, 21939–21947.

118 Y. Wu, P. Zheng, J. Peng, M. Xu, Y. Chen, S. Surve, T. Lu and A. D. Bui, *et al.*, 27.6% Perovskite/c-Si Tandem Solar Cells Using Industrial Fabricated TOPCon Device, *Adv. Energy Mater.*, 2022, **12**, 2200821.

119 Y. Chen, N. Yang, G. Zheng, F. Pei, W. Zhou, Y. Zhang, L. Li and Z. Huang, *et al.*, Nuclei engineering for even halide distribution in stable perovskite/silicon tandem solar cells, *Science*, 2024, **385**, 554–560.

120 D. Zheng, F. Raffin, P. Volovitch and T. Pauporté, Control of perovskite film crystallization and growth direction to target homogeneous monolithic structures, *Nat. Commun.*, 2022, **13**, 6655.

121 H. X. Dang, K. Wang, M. Ghasemi, M.-C. Tang, M. De Bastiani, E. Aydin, E. Dauzon and D. Barrit, *et al.*, Multi-cation Synergy Suppresses Phase Segregation in Mixed-Halide Perovskites, *Joule*, 2019, **3**, 1746–1764.

122 D. Burkitt, J. Searle, D. A. Worsley and T. Watson, Sequential Slot-Die Deposition of Perovskite Solar Cells Using Dimethylsulfoxide Lead Iodide Ink, *Materials*, 2018, **11**, 2106.

123 J. S. Yun, J. Seidel, J. Kim, A. M. Soufiani, S. Huang, J. Lau, N. J. Jeon and S. I. Seok, *et al.*, Critical Role of Grain Boundaries for Ion Migration in Formamidinium and Methylammonium Lead Halide Perovskite Solar Cells, *Adv. Energy Mater.*, 2016, **6**, 1600330.

124 Q. Fan, Y. Cui, Y. Li, J. A. Vigil, Z. Jiang, P. Nandi, R. Colby and C. Zhang, *et al.*, Phase segregation dynamics in mixed-halide perovskites revealed by plunge-freeze cryo-electron microscopy, *Cell Rep. Phys. Sci.*, 2025, **6**, 102653.

125 M. Dailey, Y. Li and A. D. Printz, Residual Film Stresses in Perovskite Solar Cells: Origins, Effects, and Mitigation Strategies, *ACS Omega*, 2021, **6**, 30214–30223.

126 G. Yang, C. Deng, C. Li, T. Zhu, D. Liu, Y. Bai, Q. Chen and J. Huang, *et al.*, Towards efficient, scalable and stable perovskite/silicon tandem solar cells, *Nat. Photonics*, 2025, **19**, 913–924.

127 C. Kan, P. Hang, S. Wang, B. Li, X. Yu, X. Yang, Y. Yao and W. Shi, *et al.*, Efficient and stable perovskite-silicon tandem solar cells with copper thiocyanate-embedded perovskite on textured silicon, *Nat. Photonics*, 2025, **19**, 63–70.

128 D. Turkay, K. Artuk, M. Othman, F. Sahli, L. Champault, C. Allebé, A. Hessler-Wyser and Q. Jeangros, *et al.*, Beyond Flat: Undulated Perovskite Solar Cells on Microscale Si Pyramids by Solution Processing, *ACS Energy Lett.*, 2025, **10**, 1397–1403.

129 D. Zhang, T. Wu, B. Li, D. Ding, R. Li, J. Wei, H. Zhang and C. Kan, *et al.*, Iceberg-like pyramids in industrially textured silicon enabled 33% efficient perovskite-silicon tandem solar cells, *Nat. Commun.*, 2025, **16**, 7331.

130 R. Santbergen, M. R. Vogt, R. Mishima, M. Hino, H. Uzu, D. Adachi, K. Yamamoto and M. Zeman, *et al.*, Ray-optics study of gentle non-conformal texture morphologies for perovskite/silicon tandems, *Opt. Express*, 2022, **30**, 5608–5617.

131 Y. Li, H. Sai, C. McDonald, Z. Xu, Y. Kurokawa, N. Usami and T. Matsui, Nanoscale Size Control of Si Pyramid Texture for Perovskite/Si Tandem Solar Cells Enabling Solution-Based Perovskite Top-Cell Fabrication and Improved Si Bottom-Cell Response, *Adv. Mater. Interfaces*, 2023, **10**, 2300504.

132 S. Wang, W. Li, C. Yu, W. Shi, Q. Kang, F. Cao, K. Gao and L. Yang, *et al.*, Flexible perovskite/silicon tandem solar cells with 33.6% efficiency, *Nature*, 2026, **649**, 59–64.